Supplementary Information for

Single-cell analysis resolves the cell state transition and signaling dynamics associated with melanoma drug-induced resistance

Yapeng Su, Wei Wei, Lidia Robert, Min Xue, Jennifer Tsoi, Angel Garcia-Diaz, Blanca Homet Moreno, Jungwoo Kim, Rachel H. Ng, Jihoon W. Lee, Richard C. Koya, Begonya Comin-Anduix, Thomas G. Graeber, Antoni Ribas, James R. Heath

Y.S., W.W., L.R. contributed equally to this work.

Correspondence: W.W. weiwei@mednet.ucla.edu; A.B. aribas@mednet.ucla.edu; and J.R.H. heath@caltech.edu

Supplementary Materials and Methods

Cell lines, reagents and cell culture

Human melanoma cell lines (M series) were established from patient's biopsies under UCLA IRB approval # 11–003254. Cells were cultured in RPMI 1640 with L-glutamine (Mediatech, Inc, Manassas, VA), 10% fetal bovine serum (Omega Scientific Tarzana, CA), and 1% penicillin, streptomycin and fungizone (Omega Scientific Tarzana, CA). Cultures were incubated in a water-saturated incubator at 37°C with 5% CO_2. Cells were maintained and tested for mycoplasma as described before (1, 2). Cell lines were periodically authenticated to their early passages using GenePrint® 10 System (Promega, Madison, WI). Presence of mutations in the genes of interest was checked by OncoMap 3 or Iontrone, and was confirmed by PCR and Sanger sequencing as previously described (1, 2).

Vemurafenib (NC0621949, Selleck Chemicals LLC), trametinib (NC0592237, Selleck Chemicals LLC), and JSH-23 (S7351, Selleck Chemicals LLC) were dissolved in DMSO at designated concentrations before applying to cell culture media. All cell lines were plated in T-75 plates at 60% confluency and treated with vemurafenib at twice the 50% inhibition concentration ($2 \times IC_{50}$) of each cell line using their previously described IC_{50} (Table S1). The DNA-antibody conjugates were synthesized with previous protocols reported (3). The list of ssDNA and antibodies used in this work is shown in Tables S6 and S7.

Phenotype tracking by flow cytometry.

Cell suspensions were stained for flow cytometry with PE conjugated anti human NGFR antibody from Biolegend (San Diego, CA). All cells were then fixed with Fix-Perm buffer from BD Bioscience (San Jose, CA) and stained for intracellular FITC conjugated anti human Melan-A antibody from Santa Cruz (Dallas, TX). Isotypes for mouse IgG1k and mouse IgG1 respectively were used to enable correct gating and to confirm antibody specificity. Blue live-dead staining from Life technologies (Waltham, MA) was used to discriminate alive. 10000 alive events were collected for each sample. Flow cytometry analysis was conducted using LSR-II from BD Biosciences (San Jose, CA), and the data was analyzed using FlowJo software (Tree Star, Inc., San Carlos, CA). The hierarchical clustering from the 18 cell lines, was performed using the expression levels in flow cytometry, with complete linkage and Euclidean distance metric. Gating of NGFR and Mart1 for defining cell states are all based on the staining of isotype controls.

MITF Reporter Cell Line

The human *Tyrosinase Promoter* (TP) was subcloned from pLightSwitch Prom S700747 (SwitchGear Genomics, Carlsbad, CA), which was first digested with MluI (New England Biolabs; Ipswich, MA). Blunt ends were generated using T4 Polymerase (New England Biolabs) and the resulting fragment was digested again with Bgl II (New England Biolabs). Resulting 1057 bp Tyrosinase promoter insert was then cloned by standard methods (4) into the BamH1 and HpaI sites of the lentiviral vector backbone Lenti-D-EN-fLUC, driving the expression of the firefly luciferase gene.

Lentivirus particles were generated as previously described (5) to stably transduce M229, M263 and M397. Generated stable reporter cell lines M229TP, M263TP and M397TP from different conditions were trypsinized and seeded at a density of 100.000 cells per well in 96-well white-bottomed plates. Luciferase activity was read out from white-bottomed plates using luciferin directly (1:10 Final dilution) and signal was normalized according to viability calculated using CellTiter-Glo (Promega, San Luis Obispo, CA) (1:2 final dilution), also plated in white-bottomed plates. Bioluminescence imaging was carried out with a Xenogen IVIS 200 Imaging System (Xenogen/Caliper Life Sciences).

RNA-Seq

RNA extraction was performed using AllPrep DNA/RNA Mini kit from Qiagen in 18 human melanoma cell lines samples and also in samples from M229, M263 and M397 treated under different conditions. Bioanalyzer confirmed correct integrity, library was constructed and Illumina 50 bp single-end RNA-seq data was collected for the samples described. RNA sequencing was performed using 50 bps single end sequencing on the Illumina HiSeq 2500 platform. Libraries were prepared using the IlluminaTruSeq RNA sample preparation kit per the manufacturer's instructions. Reads were mapped and aligned to the Homo sapiens NCBI build 37.2 reference genome using TopHat2 v2.0.9(6). Expression values in fragments per kilobase of exon per million fragments mapped (FPKM) were generated using Cufflinks v2.2.1 program and Cuffnorm to quantify and normalize aligned reads using the geometric library size normalization method (7).

The stochastic cell transition model

The stochastic cell-state transition model is built by assuming a time-homogeneous Markov chain process as described in a previous publication (8). Two basic assumptions are made for the model: First, cells at four designated subpopulations transition randomly between states per certain unit time. Second, the transition probabilities depend only on a cell's current state, regardless of its prior states. The governing equations are listed below.

$$\begin{bmatrix} \text{original} \\ \text{proportions} \end{bmatrix} \left[\begin{bmatrix} \text{treatment} \\ \text{sensitivity matrix} \end{bmatrix} \begin{bmatrix} \text{State transition} \\ \text{probability matrix} \end{bmatrix} \right]^{\text{Time}} = \begin{bmatrix} \text{new} \\ \text{proportions} \end{bmatrix}$$

Proportions of various states are listed as column vectors. The 4×4 state transition probability matrix with each element denoting the transition probability from one cell state to other states per unit time is pre-multiplied with a diagonal drug sensitivity matrix. The four diagonal elements of this matrix encode the relative viability of the two melanocyte, neural crest and double negative states in the presence of drug treatment. The calculated 4-element vector is normalized to have a summation of 1 to generate the new proportions vector.

Kinetic flow cytometry data (Table S5) of segregated cell populations at different time points are used as input. Monte Carlo simulation is performed by random sampling differential transition probability and viability vectors to quantitatively infer the most probable values in the matrices that best recapitulate the experimental observations of sorted cells. The values inferred from sorted cells are then utilized to predict the cell state dynamics and final steady-state composition of unsorted cells under drug treatment (Fig. 2D).

Transcriptomic data analysis

Heatmap and clustering analysis of transcriptomic dataset for all 9 cell lines was performed via MATLAB. Genes are pre-filtered by RPKM value with criteria of average value greater than1 and coefficient of variance greater than 0.3. Filtered gene expression values were standardized across each row (normalized for each individual gene) and represented by redblue colormap. Hierarchical clustering was performed with average linkage and Euclidean distance metric. Whole transcriptomic dataset for each cell line upon drug treatment was also plotted as self-organized mosaic maps with respective to its control via Gene Expression Dynamics Inspector (GEDI) (9). Each tile in the maps represents a minicluster of genes with similar expression kinetics. Gene clusters with related expression kinetics are placed close together, while clusters exhibiting very different kinetic trajectories are placed far apart. The tile color encodes the average expression level of the genes in that minicluster at a given time point. By extracting genes in interesting regions (e.g. common regions that are changing in the same direction across all cell line clusters or unique regions that are only changing in only one cluster, *etc.*), one could further investigate their biological functions. Genes in regions of interest are further enriched in the Gene Ontology Biology Process database using Enricher (10).

For generating the phenotypic trajectory in Figs. 1D and S4, the MITF activity and neural crest signature scores were determined by using genes identified as MITF targets (11) and chicken embryo neural crest genes from Gallus EST in situ hybridization analysis – GEISHA- (12) (Table S3) respectively. Signatures scores were calculated by taking the sum of all log2 fold changes from DMSO control for all signature genes and divided by the square root of the total number of genes.

Gene Set Enrichment Analysis (GSEA) was performed using GSEA v2.2.3 software with 1000 permutations and weighted enrichment statistics. For correlation enrichment, we used Pearson correlation of relevant pathways with *MITF, L1CAM, NGFR, NFκB1, CCL2,* and *AXL* expression across patient samples. For the pre-ranked option with $\log_2$ fold changes were used as the ranking metric. Normalized enrichment score (NES) was assessed across the curated Molecular Signatures Database (MSigDB) Hallmark, C2 curated gene sets, and MITF signature (11).

Using Database for Annotation, Visualization and Integrated Discovery (DAVID) 6.8, we looked at relevant Gene ontology (GO) terms for differentially expressed genes for M229, M263 and M397 at 21 days and 73-90 days of drug treatment with respect to DMSO control (Fig. S7).

Microchip fabrication and single cell proteomic assay

The fabrication of the SCBC devices and the protocol of the single cell proteomic assays were extensively discussed in our previous publications (13, 14). Briefly, the DNA microarrays at each microchamber were converted to antibody microarrays by flowing the DNA-antibody conjugate cocktail solution immediately prior to use. Cells were randomly loaded into the 310 microchambers of the SCBC. Each microchamber has an assay component, and a separate reservoir of lysis buffer, and was photographed after cell loading. The SCBC was then cooled on ice for cell lysis. Following a 2-hour protein capture period at room temperature, the microchambers were flushed and the antibody arrays were developed using a cocktail of detection antibodies. The developed antibody barcode arrays were digitized by a Genepix

scanner. Each array is matched with the micrograph of that array for preparing a table that contains the microchamber address, the numbers of cells, and the measured fluorescence levels of each assayed protein.

Clonogenic assay

Clonogenic assays were performed by plating melanoma cells in six-well plates with fresh media at an optimal confluence. The media (with drug or DMSO) were replenished every 2 days. Upon the time of staining, 4% paraformaldehyde was applied onto colonies to fix the cells and 0.05% crystal violet solution was used for staining the colonies.

Drug dose-response SRB assay

The 3 cell lines were pre-seeded into 96-well plates for 48 hours before the addition of drug. After that, cells were treated with drug for 72 hours, and cell viability was determined using In Vitro Toxicology Assay Kit (TOX6, SIGMA-ALDRICH) following the manufacturer's instruction. A Bliss independence model was used to evaluate the effect of drug combination (15).

Statistical analysis of SCBC data

The SCBC readouts from the microchambers with a single cell were collected to form a data table. Each row of the table corresponds to a measurement of a panel of functional proteins from a single cell and each column contains digitized fluorescence intensities that provide readout of the levels of each of the assayed proteins. Protein-protein Spearman’s rank correlation coefficients can be directly calculated from single cell data. Protein correlation networks were generated by running the calculation through all the protein pairs in panel (Fig. S12). Bonferroni corrected p-value was used to define the statistical significance level for the entire panel and only those significant correlations were shown in the networks.

The t-SNE dimensionality reduction analysis was performed on SCBC dataset following a previous published algorithm (16).

A normalized PCA was used to peel off layer after layer of systematic co-variations from the data, in terms of principal components (PCs). The correlations between functional protein levels and PCs were calculated to quantify the dominative protein pattern of the signaling network coordination and its response to external perturbations such as drug treatment. The signaling network activity index (SNAI) is a metric of the overall strength of the protein signaling coordination at a given condition, and is defined as the reciprocal of the determinant of the protein-protein correlations.

Supplementary References

1. Wong DJ*, et al.* (2014) Antitumor activity of the ERK inhibitor SCH772984 [corrected] against BRAF mutant, NRAS mutant and wild-type melanoma. *Mol Cancer* 13:194.
2. Atefi M*, et al.* (2014) Effects of MAPK and PI3K pathways on PD-L1 expression in melanoma. *Clin Cancer Res* 20(13):3446-3457.
3. Bailey RC, Kwong GA, Radu CG, Witte ON, & Heath JR (2007) DNA-encoded antibody libraries: a unified platform for multiplexed cell sorting and detection of genes and proteins. *J Am Chem Soc* 129(7):1959-1967.
4. Green MR, Sambrook J, & Sambrook J (2012) *Molecular cloning : a laboratory manual* (Cold Spring Harbor Laboratory Press, Cold Spring Harbor, N.Y.) 4th Ed.
5. Koya RC*, et al.* (2010) Kinetic phases of distribution and tumor targeting by T cell receptor engineered lymphocytes inducing robust antitumor responses. *Proc Natl Acad Sci U S A* 107(32):14286-14291.
6. Kim D*, et al.* (2013) TopHat2: accurate alignment of transcriptomes in the presence of insertions, deletions and gene fusions. *Genome Biol* 14(4):R36.
7. Trapnell C*, et al.* (2010) Transcript assembly and quantification by RNA-Seq reveals unannotated transcripts and isoform switching during cell differentiation. *Nat Biotechnol* 28(5):511-515.
8. Gupta PB*, et al.* (2011) Stochastic state transitions give rise to phenotypic equilibrium in populations of cancer cells. *Cell* 146(4):633-644.
9. Eichler GS, Huang S, & Ingber DE (2003) Gene Expression Dynamics Inspector (GEDI): for integrative analysis of expression profiles. *Bioinformatics* 19(17):2321-2322.
10. Chen EY*, et al.* (2013) Enrichr: interactive and collaborative HTML5 gene list enrichment analysis tool. *BMC Bioinformatics* 14:128.
11. Hoek KS*, et al.* (2008) In vivo switching of human melanoma cells between proliferative and invasive states. *Cancer Res* 68(3):650-656.
12. Bell GW, Yatskievych TA, & Antin PB (2004) GEISHA, a whole-mount in situ hybridization gene expression screen in chicken embryos. *Dev Dyn* 229(3):677-687.
13. Shi Q*, et al.* (2012) Single-cell proteomic chip for profiling intracellular signaling pathways in single tumor cells. *Proc Natl Acad Sci U S A* 109(2):419-424.
14. Xue M*, et al.* (2015) Chemical methods for the simultaneous quantitation of metabolites and proteins from single cells. *J Am Chem Soc* 137(12):4066-4069.
15. Borisy AA*, et al.* (2003) Systematic discovery of multicomponent therapeutics. *Proc Natl Acad Sci U S A* 100(13):7977-7982.
16. AD A*, et al.* (2013) viSNE enables visualization of high dimensional single-cell data and reveals phenotypic heterogeneity of leukemia. . *Nature Biotechnology* 31:545-552.

Supplementary Figures

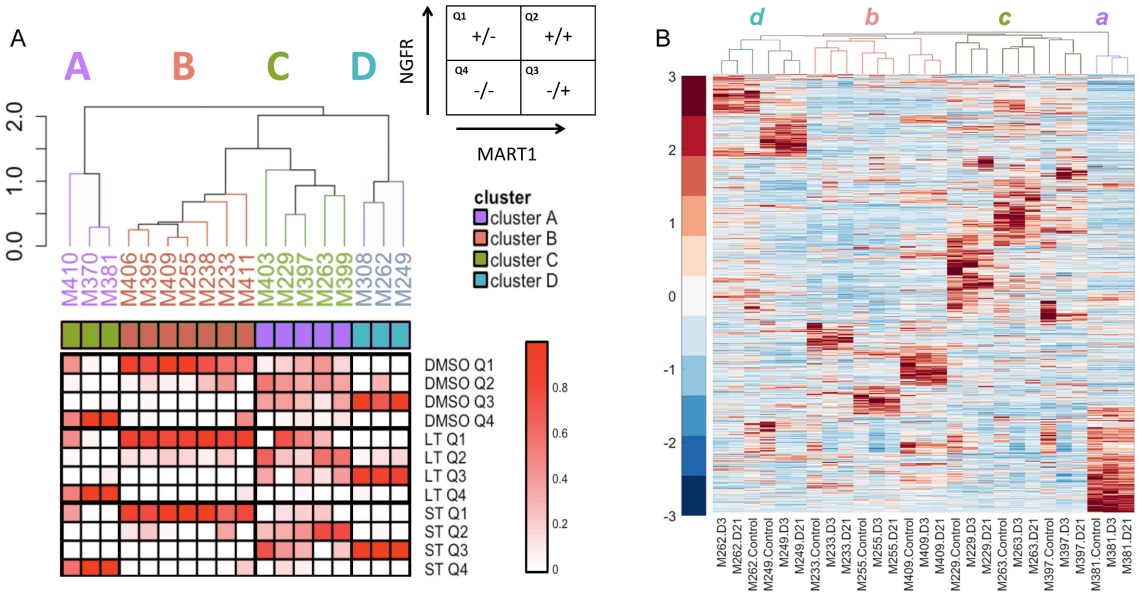

Fig. S1. Phenotypic clustering of 18 *BRAF*^{V600} mutant melanoma cell lines upon BRAF inhibition. (A) Clustering of 18 cell lines based upon their partition percentages (color coded in red) in four phenotypic quadrants (inset) at baseline and upon BRAFi response identifies 4 groups. The quadrants are defined by the gate setting of NGFR and MART-1 expression levels for each cell line in the flow cytometry analysis. Cluster C cells show highest phenotypic plasticity upon BRAF inhibition. Hierarchical clustering is performed with complete linkage and Euclidean distance metric (ST: 3 days vemurafenib treatment, LT: 3 weeks vemurafenib treatment). (B) Heat map of the genome-wide expression levels of 9 cell lines randomly selected from each cluster at control, 3 days, and 3 weeks vemurafenib treatment. Clustering is performed with average linkage by Euclidean distance metric. Four clusters are identified to be wholly consistent with the clustering results using MART-1 and NGFR markers in panel A. The clusters are labeled in lower case font, indicating that these cells represent a subset of those analyzed in panel A. Up-regulated genes are colored in red and down-regulated genes in blue.

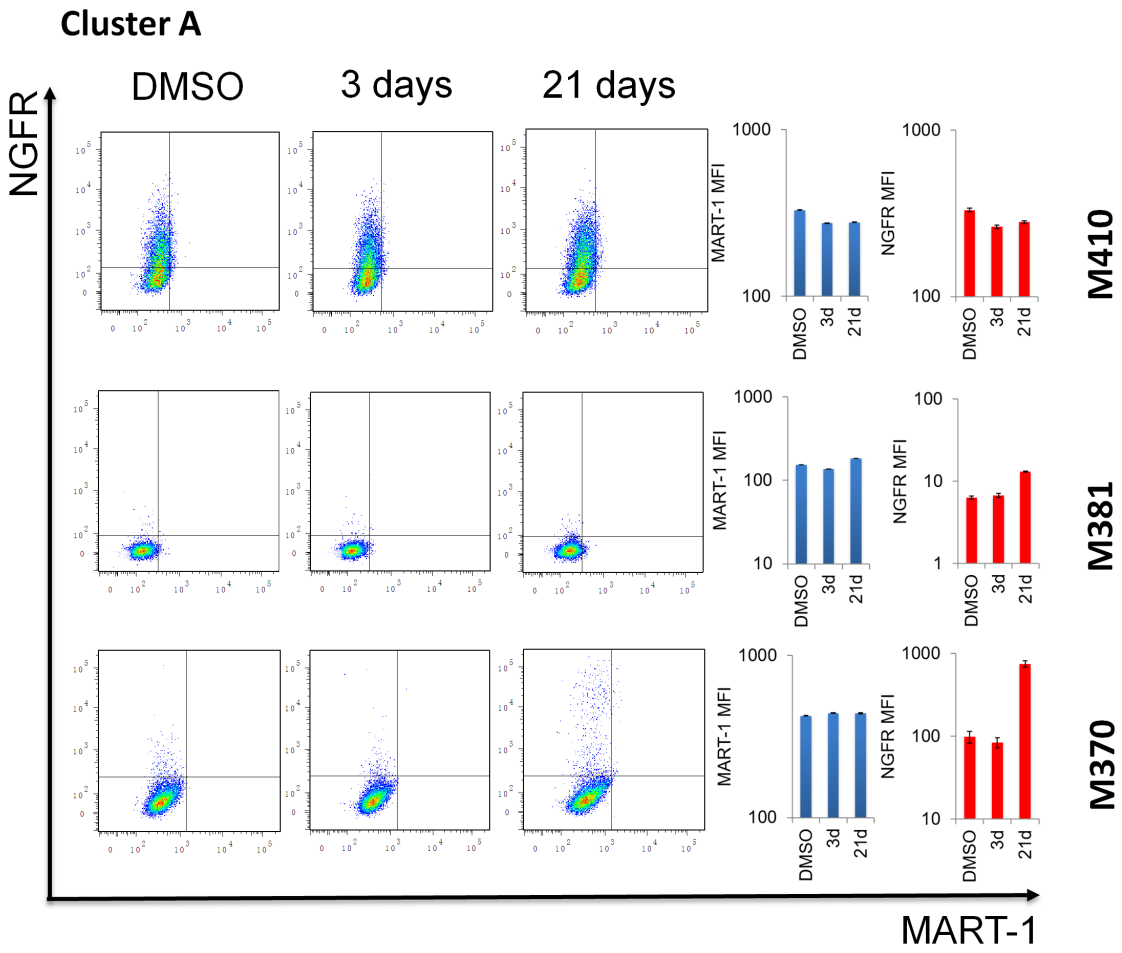
Cluster A
DMSO
3 days
21 days
NGFR
MART-1
MART-1 MFI
NGFR MFI
1000
100
10
1
DMSO
3d
21d
M410
M381
M370

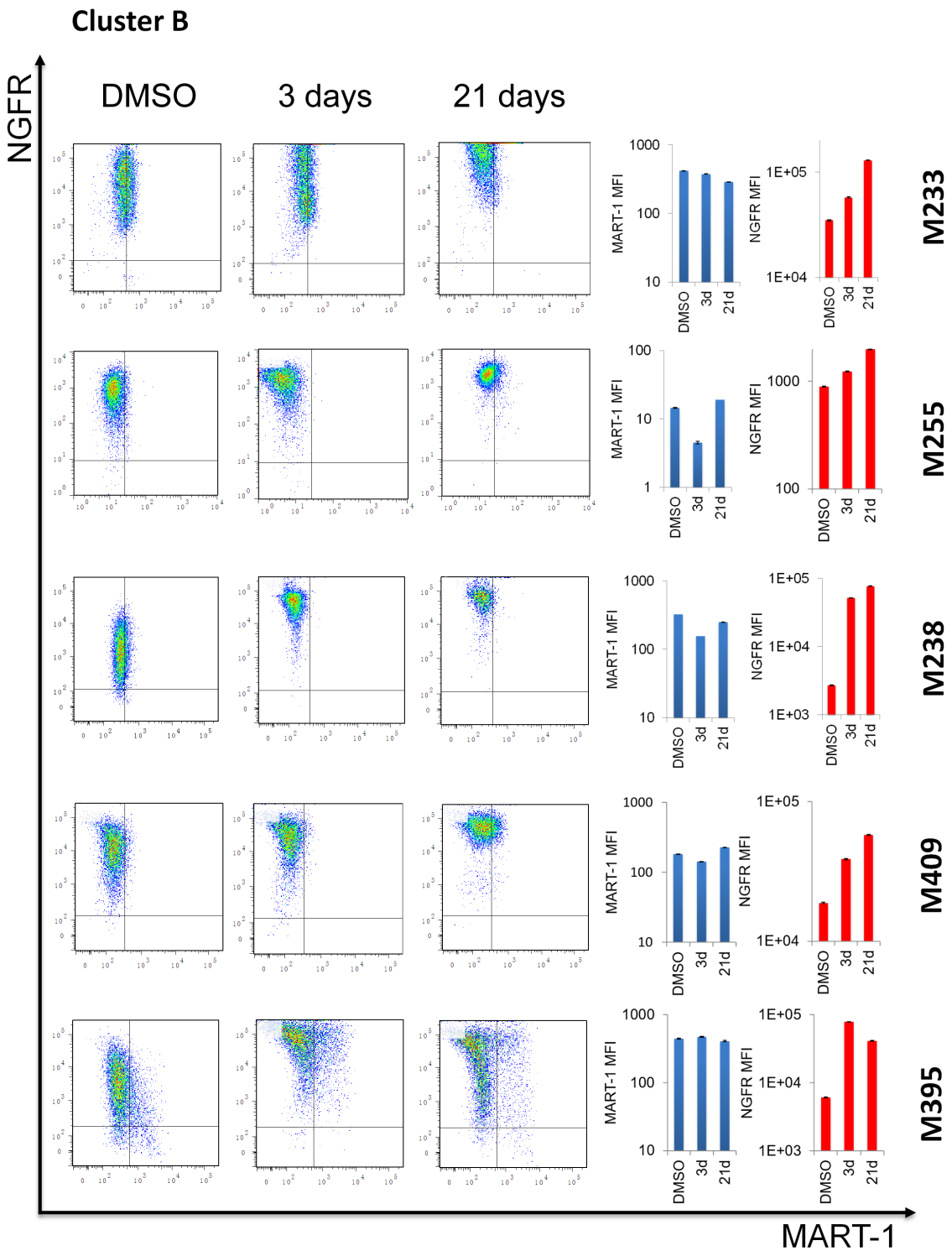
Cluster B
DMSO
3 days
21 days
NGFR
MART-1
MART-1 MFI
NGFR MFI
DMSO
3d
21d
M233
M255
M238
M409
M395

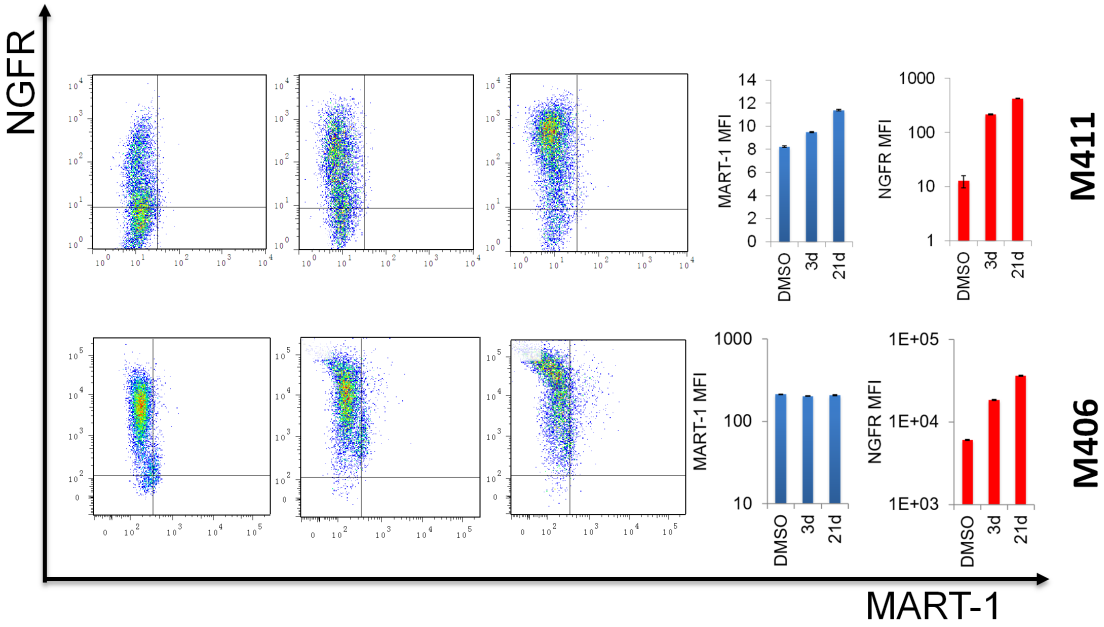
NGFR
MART-1
MART-1 MFI
NGFR MFI
DMSO
3d
21d
M411
M406

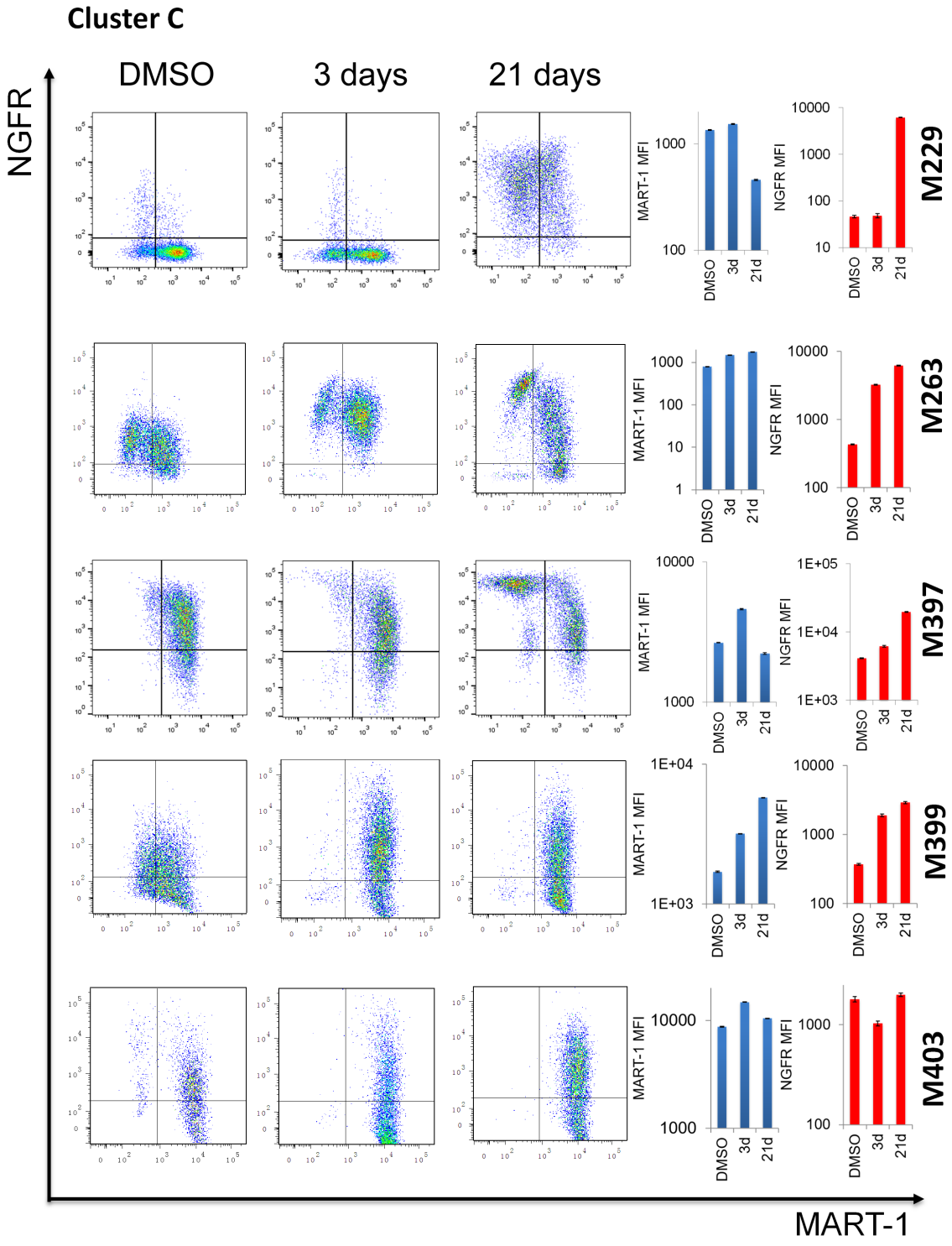
Cluster C
DMSO
3 days
21 days
NGFR
MART-1
MART-1 MFI
NGFR MFI
DMSO
3d
21d
M229
M263
M397
M399
M403

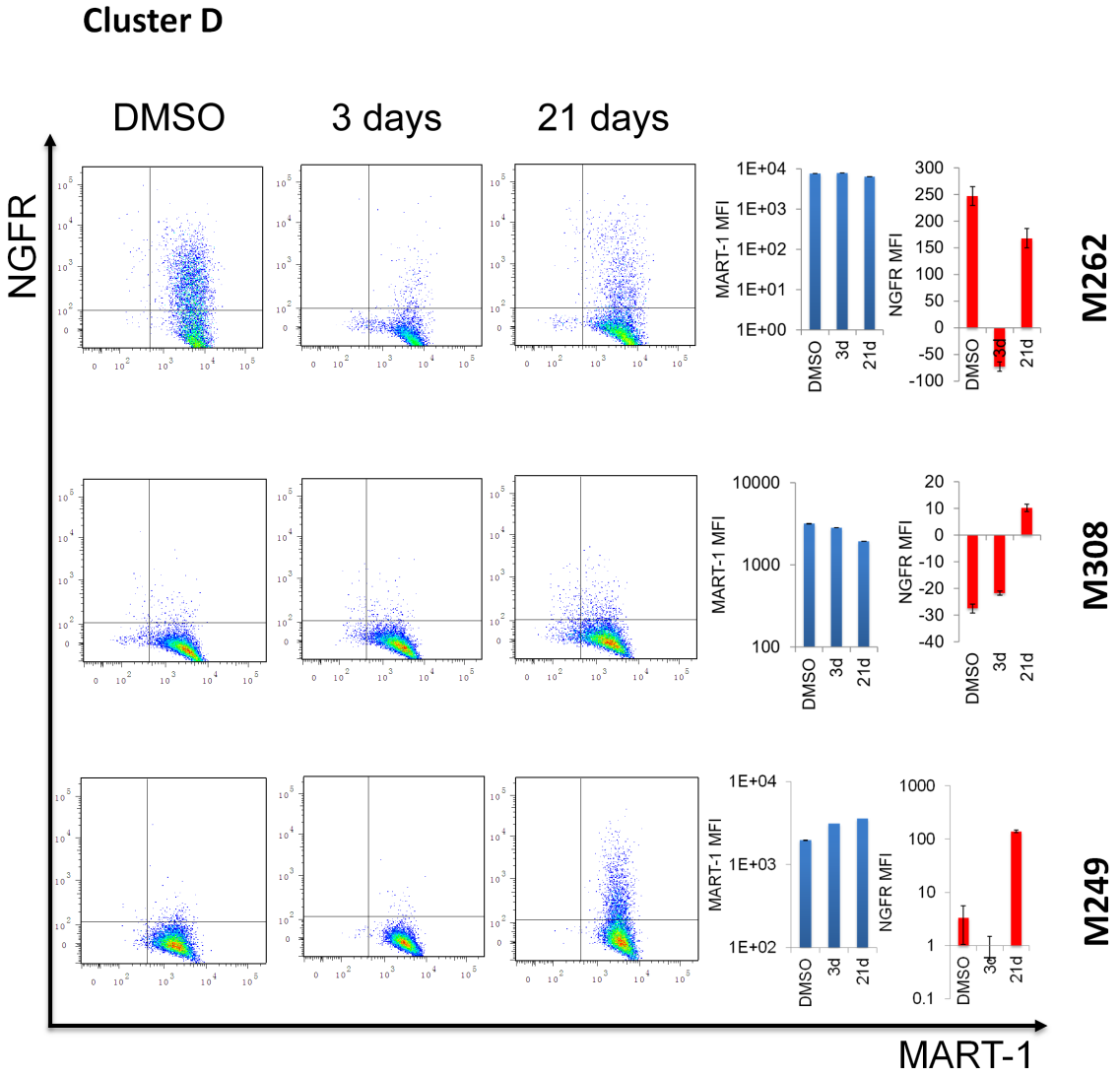

Fig. S2. Flow cytometry analysis of NGFR and MART-1 expression levels for 18 *BRAF*^{V600} mutant melanoma cell lines treated with DMSO control and vemurafenib for 3 days and 21 days. The average NGFR and MART-1 levels across treatment conditions are as bar graphs on the right (mean ± SEM). The cell lines are ordered according to the their respective clusters identified in Fig. S1A.

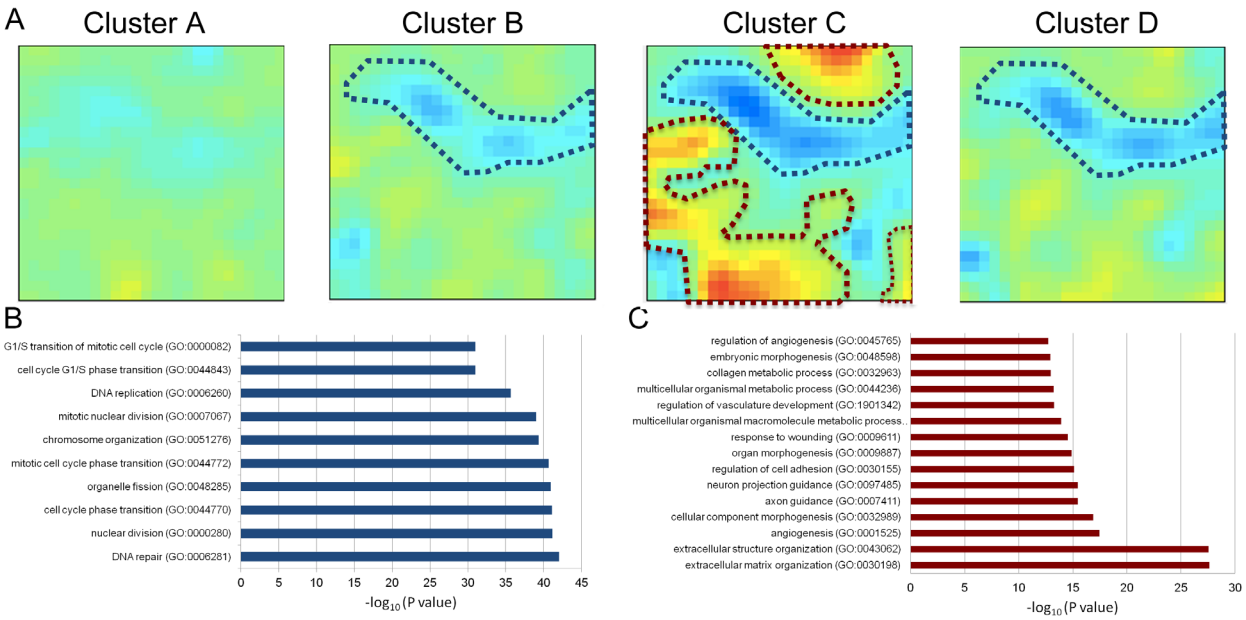

Fig. S3. Enrichment analysis of commonly down-reglated genes across all the cell line clusters and uniquely up-regulated genes in cluster C upon BRAFi exposure. (A) GEDI visualization of differentially expression genes relative to control for all the cell line clusters upon 21 days of vemurafenib treatment. Gene miniclusters circled in blue denote commonly down-regulated genes across all the cell line clusters at varying degrees. Gene miniclusters circled in red denote genes that are uniquely up-regulated in Cluster C cells. (B and C) Gene Ontology enrichment using Enricher for genes circled in blue (or red). The top 10 ontology terms with highest enrichment scores are listed from top to buttom with decreasing p values.

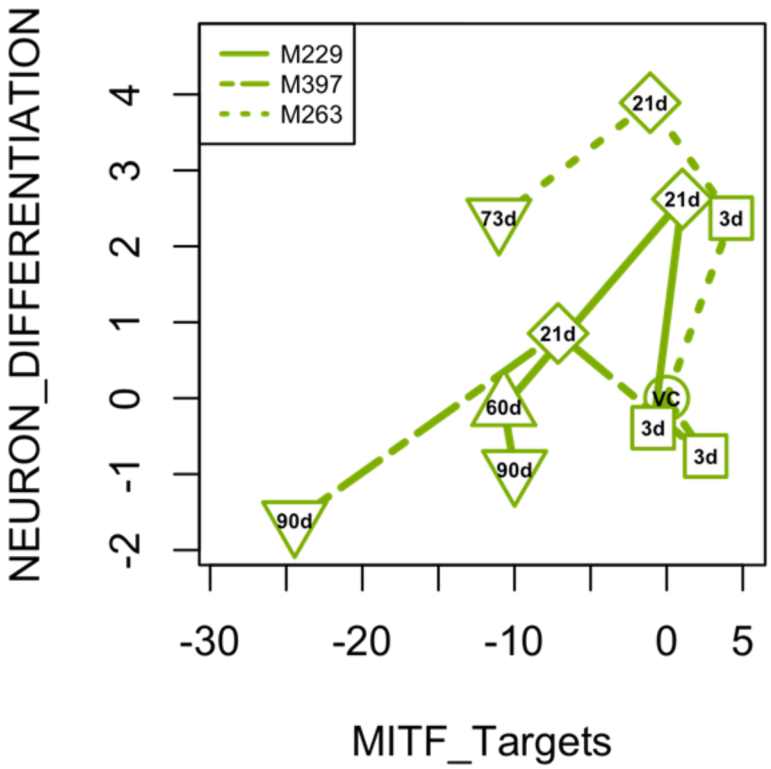

Fig. S4. Plot of MITF activity signature scores *vs* neuron differentiation (Molecular Signatures Database C5 Collection) signature scores for the 3 plastic cell lines across different time points upon vemurafenib treatment. Counterclockwise trajectories appear for all three lines (VC: DMSO control).

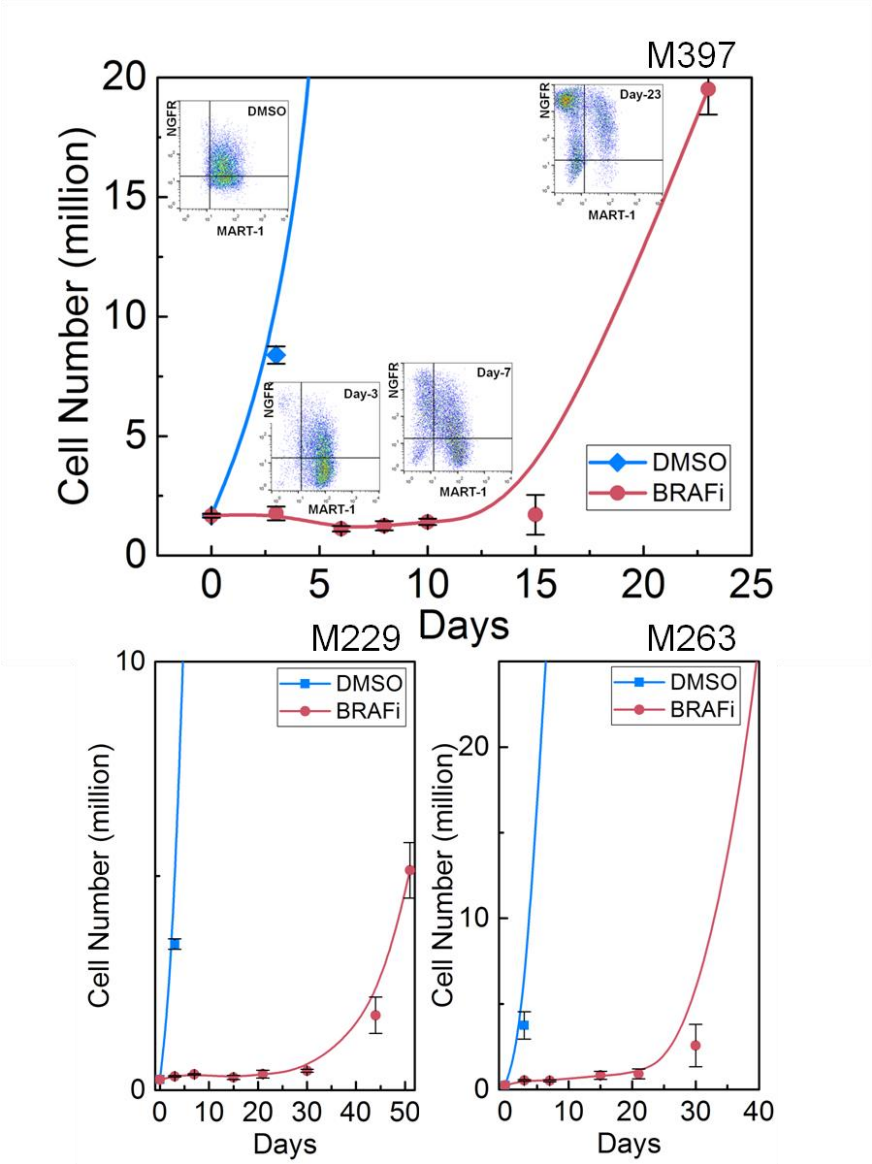

Fig. S5. Cell growth kinetics of M397, M229 and M263 under DMSO control or BRAFi treatment overlaid with phenotypic profiles (M397 only). BRAFi exposure moderately inhibited the cell growth for a short-term followed by a drug tolerant exponential growth phase characteristic of the adaptive resistance to BRAFi (data are shown as mean ± SD)

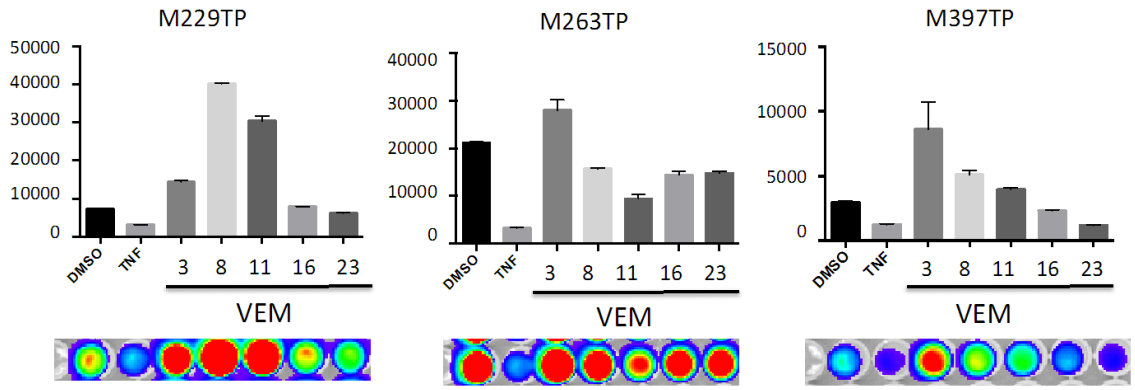

Fig. S6. MITF activity analyzed using a bioluminescence tyrosinase promoter (TP) reporter system through different time points of vemurafenib for M229TP, M263TP and M397TP. Each condition is normalized for 100,000 cells and viability. Data is representative of duplicate wells, and representative of an experiment done in two independent experiments. Error bars are standard deviation of the two wells. Luciferase representative images are shown underneath.

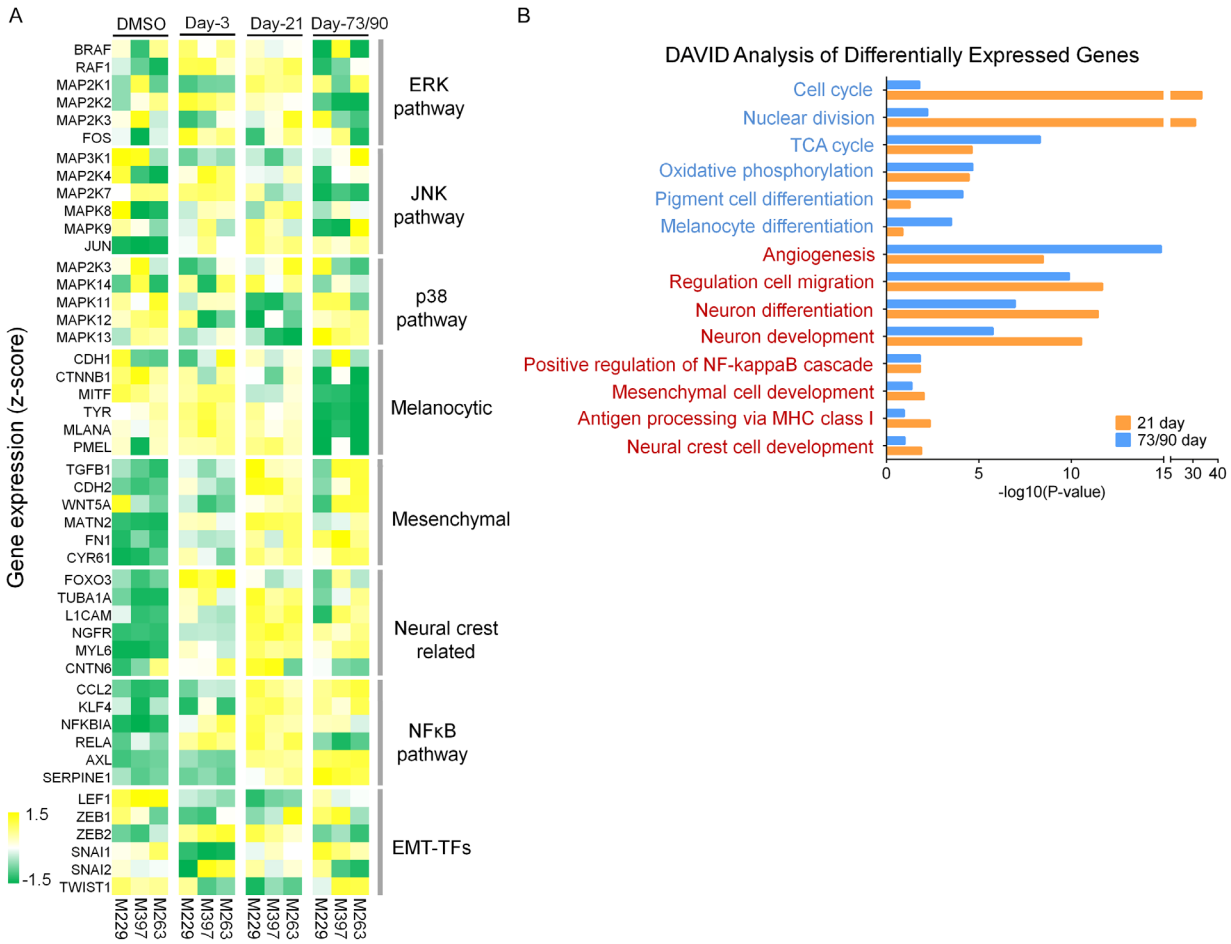

Fig. S7. Transcriptional signatures of three plastic cell lines in Cluster C. (A) Heat map of expression levels for critical genes involved in the adaptive BRAFi resistance at baseline (DMSO) as well as upon 3 days, 21 days and 73-90 days of vemurafenib exposure. (B) Gene Ontology analysis of differentially expressed genes for the three plastic cell lines following 21 days and 73-90 days drug treatment with respect to DMSO control. Relevant GO terms are listed with respective p-values, analyzed by DAVID. Blue terms denote GO term enrichment for down-regulated genes and red terms denote GO term enrichment for up-regulated genes.

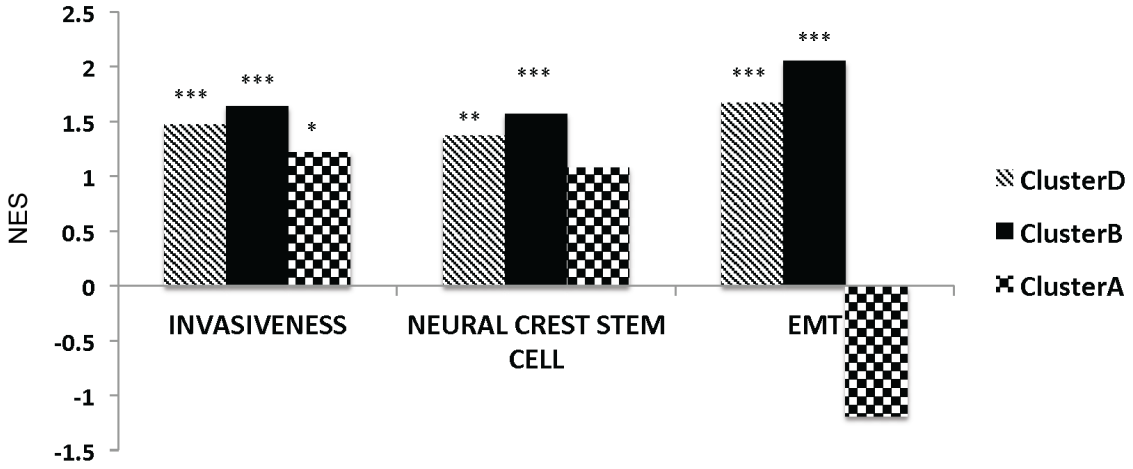

Fig. S8. GSEA shows enrichment of curated gene sets associated with the cell state regression towards neural-crest like and mesenchymal-like states upon 21 days vemurafenib exposure in other cell line clusters (NOM p values: **p<0.05; **p<0.005, ***p<0.0005*).

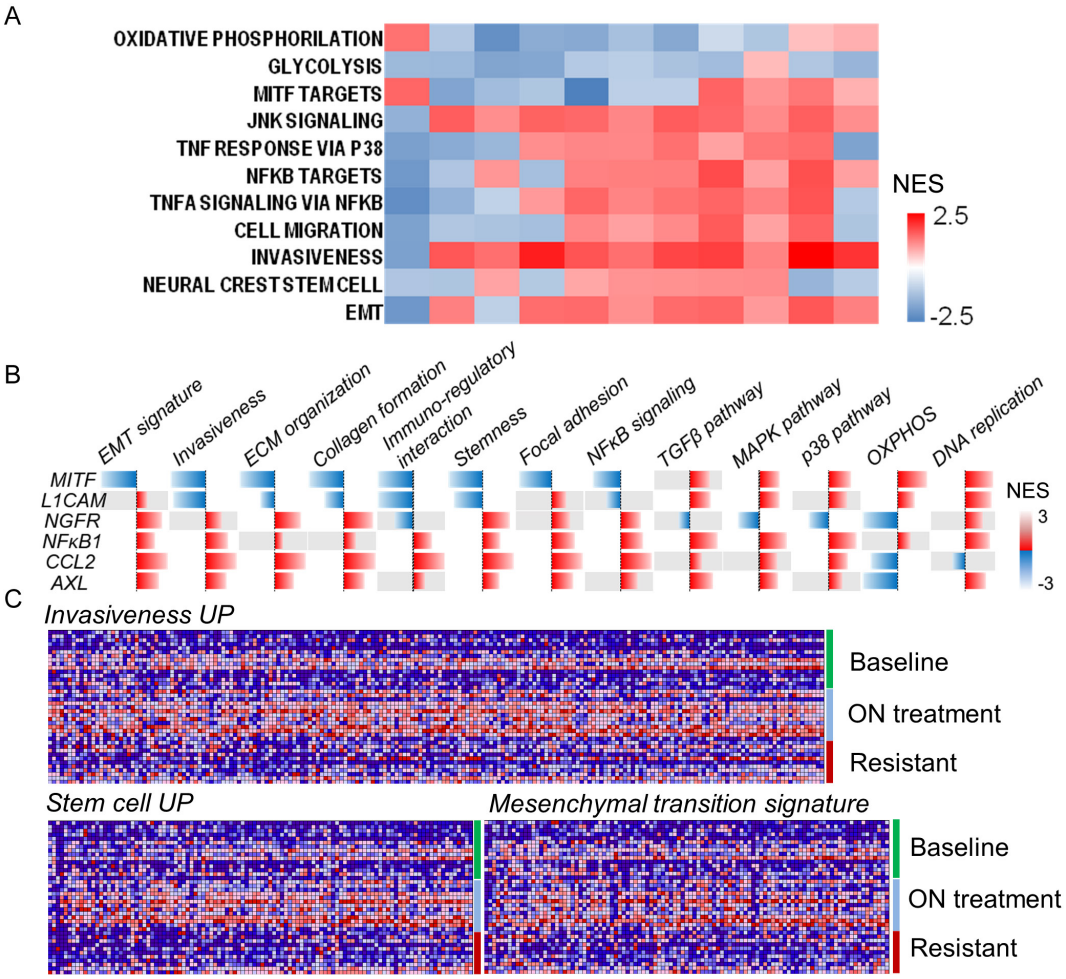

Fig. S9. Transcriptional signatures of the cell state transition associated with the adaptive resistance in melanoma patient biopsies (transcriptomes from ref. 16 in the main text). (A) Heat map of GSEA normalized enrichment scores (NES) of relevant curated gene sets involved in the adaptive transition for 11 paired pre-treatment and on-treatment patient biopsies. More than half of patient samples show acquisition of neural crest-like and mesenchymal phenotype signatures with up-regulated NFκB and JNK signaling as identified in the cell line studies. (B) Correlation of critical regulatory genes with relevant transcriptional signatures associated with the adaptive resistance across 39 melanoma patient biopsy samples. Genes involved in the ECM reprogramming, focal adhesion, collagen formation, stemness, EMT signatures were negatively correlated with *MITF* and positively correlated with *NGFR, NFκB, CCL2* and *AXL*. Gray shadow denotes an insignificant enrichment with a p value > 0.05. (C) Gene expression levels of patient samples at baseline (pre-treatment), on-treatment and resistant stages for three curated gene sets for invasiveness, stem cell and mesenchymal transition signatures. It revealed that the genes involved in cellular invasiveness, stem cell signature and EMT were consistently up-regulated at on-treatment stage and descending at acquired resistant stage, implying the existence of cellular regression towards neural crest-like and mesenchymal-like phenotypes as a non-genomic adaptive response in these on-treatment patient biopsies prior to the disappearance of these signatures when cells acquired robust therapy resistance potentially genetically.

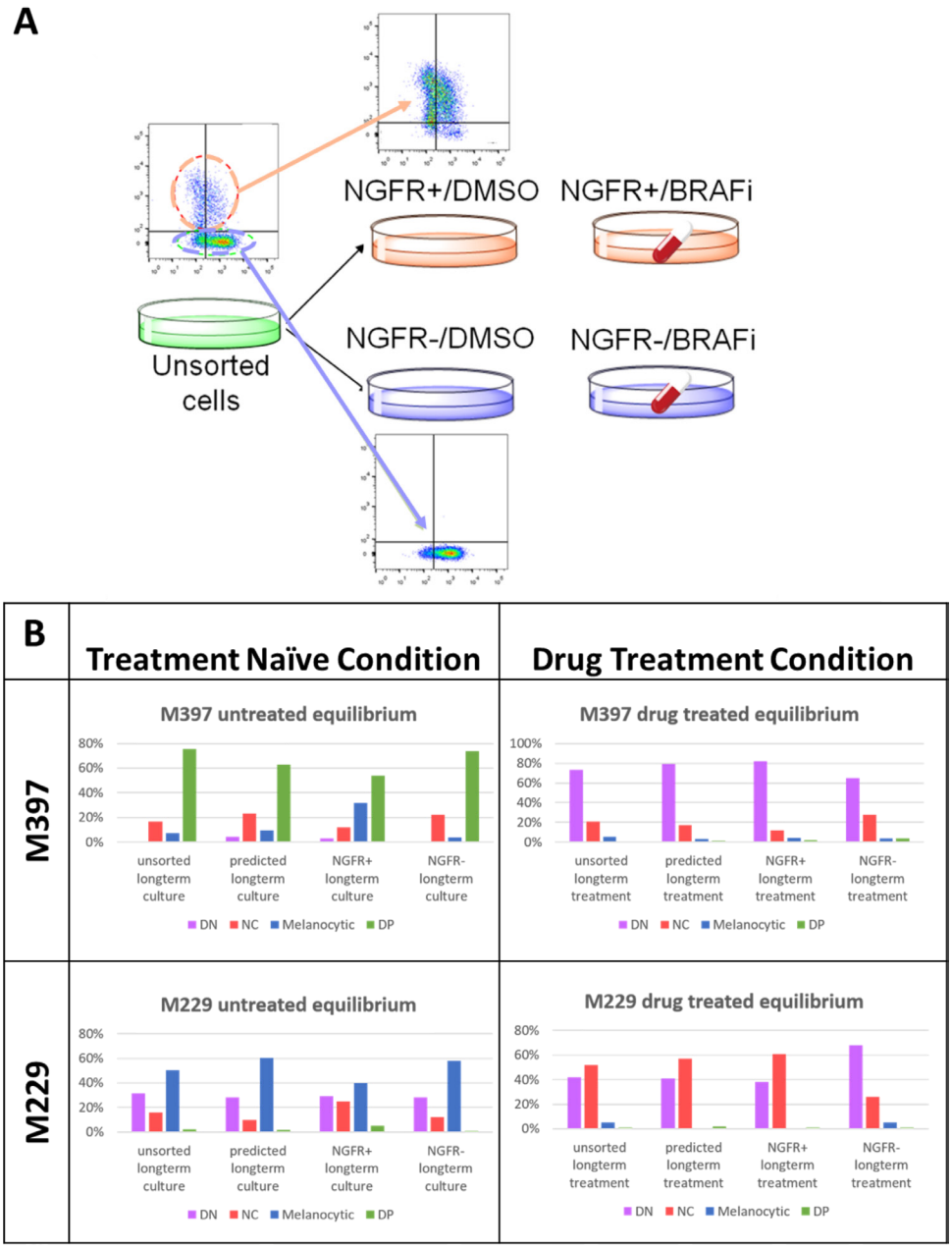

Fig. S10. The Markov model prediction and the experimental validation of cell state kinetics for segregated M229 and M397 cells. (A) Experimental flow for sorting cells to obtain NGFR+ and NGFR- subpopulations, and culturing each subpopulation in fresh growth media with or without BRAFi treatment. (B) For both M397 and M229 cell lines, unsorted cells or sorted NGFR+ or NGFR- subpopulations are cultured with or without drug, and their phenotype composition are monitored using flow cytometry until they reach to an equilibrium composition. The final equilibrium composition from unsorted, NGFR+/- subpopulations and model prediction are presented as bargraphs. DN – double negative mesenchymal-like state (NGFR-/MART-1-), NC – neural crest-like state (NGFR+/MART-1-), DP – double positive plastic state (NGFR+/MART-1+), melanocytic state (NGFR-/MART-1+).

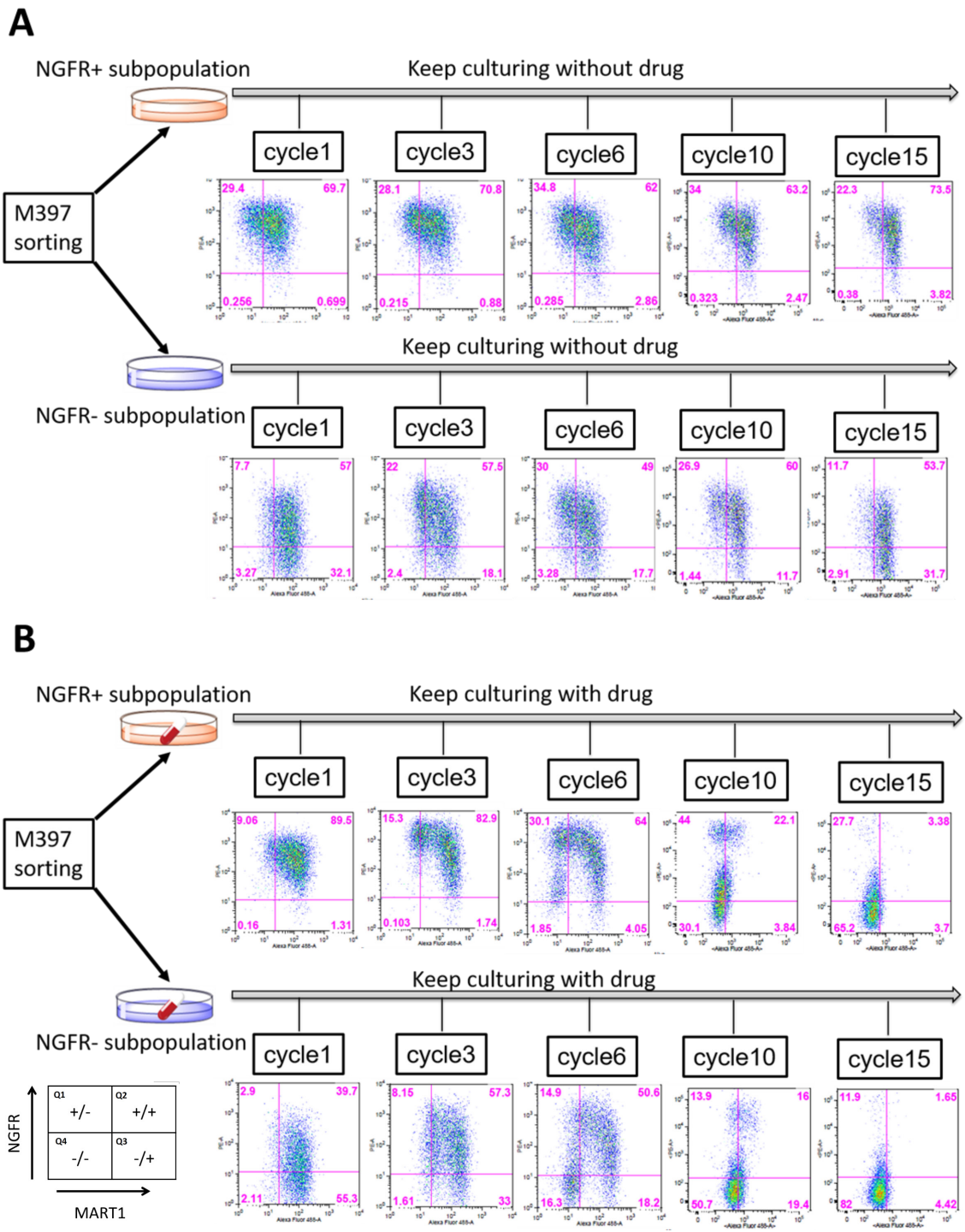

Fig. S11 Experiments setting and flow cytometry plots of sorted M397 NGFR+ and NGFR- subpopulations under treatment naïve and drug treatment conditions. Time-series flow cytometry phenotyping of M397 sorted subpopulations cultured without BRAFi (A) and with BRAFi (B) treatment. The cell cycle for M397 is 3 days.

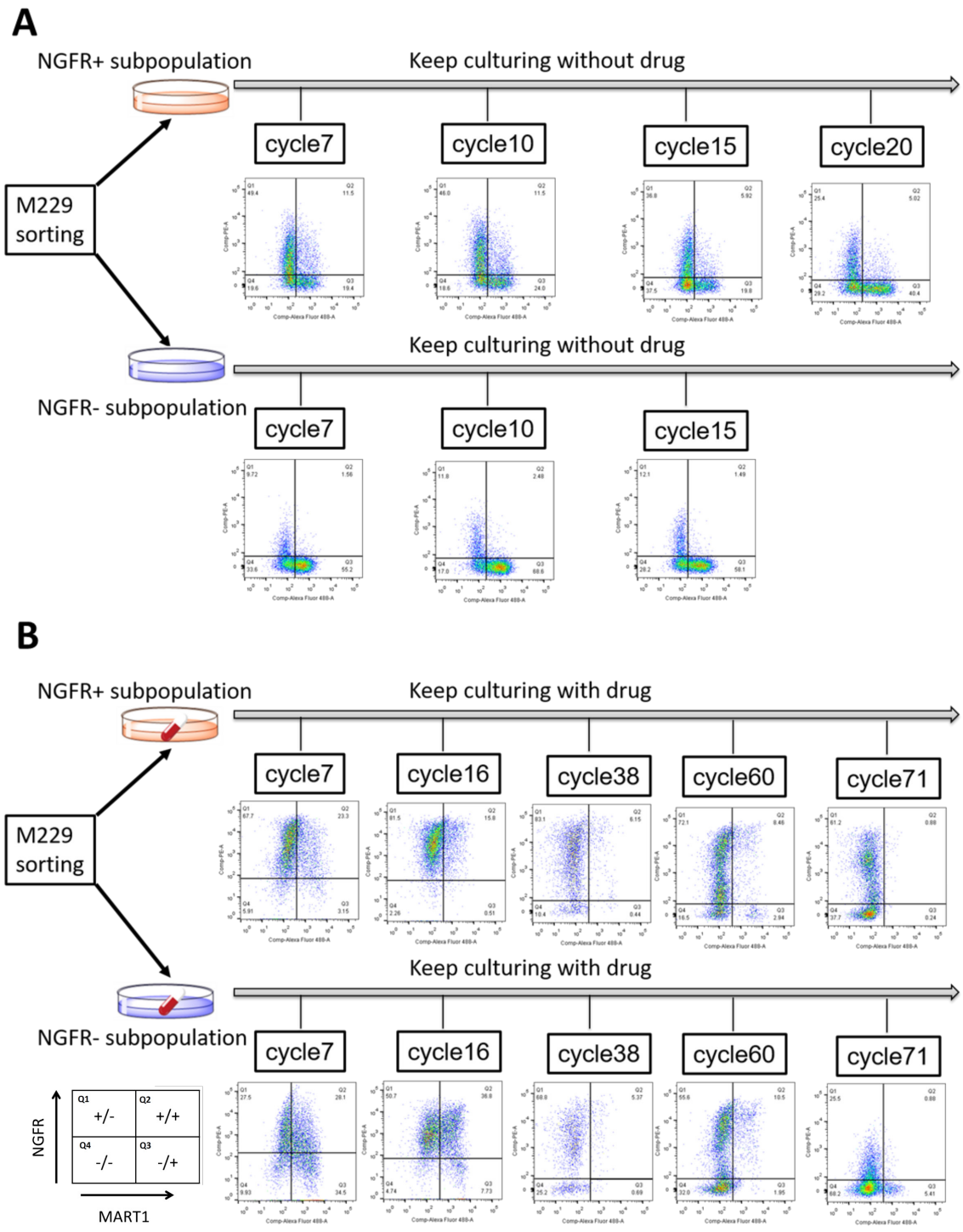

Fig. S12. Experiments setting and flow cytometry plots of sorted M229 NGFR+ and NGFR- subpopulations under treatment naïve and drug treatment conditions. Time-series flow cytometry phenotyping of M229 sorted subpopulations cultured without BRAFi (A) and with BRAFi (B) treatment. The cell cycle for M229 is 1 day.

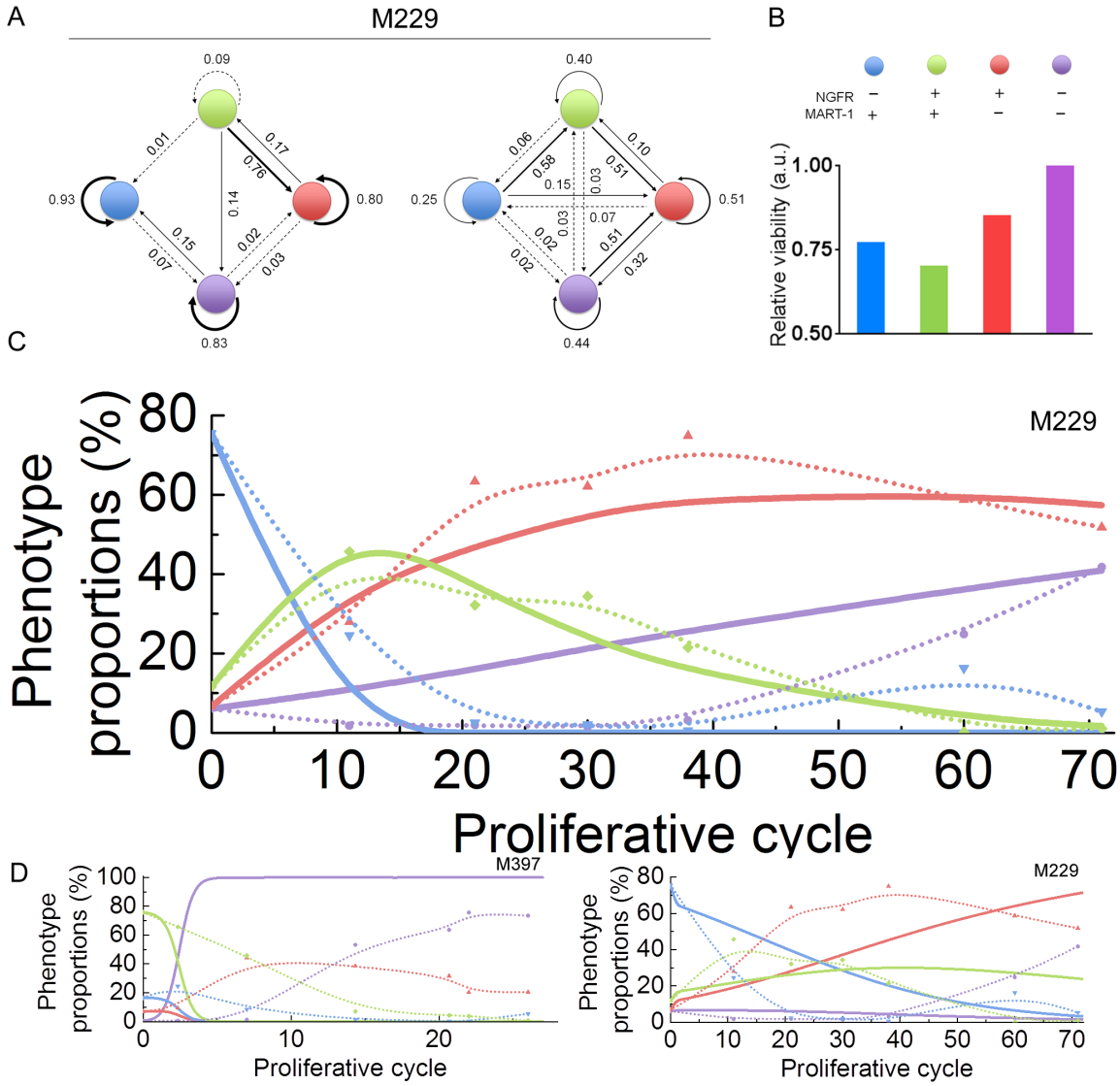

Fig. S13. Markov model of stochastic cell state transition predicts phenotypic evolution of melanoma cells upon BRAF inhibition. (A) Cell state transition probabilities of M229 at untreated and vemurafenib treated conditions. (B) Treatment sensitivity of different phenotypes for M229 inferred by the model. (C) Model prediction of the phenotypic kinetics (solid lines) versus experimental data (dots connected with dash lines) for M229 with continuous exposure to vemurafenib. (D) Model prediction of the phenotypic kinetics (solid lines) versus experimental data (dots connected with dash lines) for M397 and M229 when only drug selection is considered.

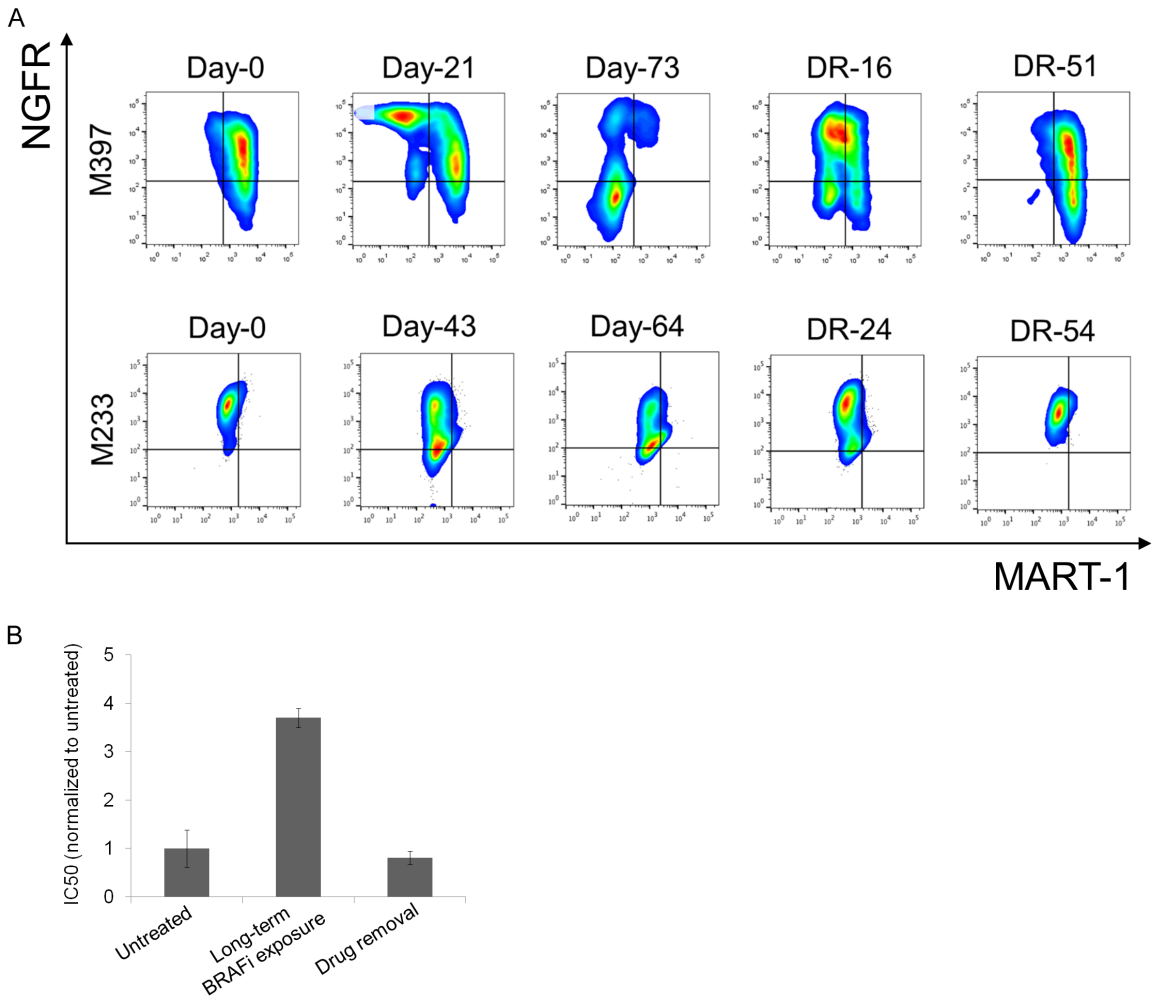

Fig. S14. Reversibility of the adaptive transition upon drug removal (A) Phenotypic reversibility for the plastic M397 cell line in Cluster C and less plastic M233 cell line in Cluster B. While starting at different baseline phenotypic composition, both M397 and M233 cell lines follow the transition trajectory towards double negative state (NGFR-/MART-1-) upon drug exposure and return to their original composition upon drug removal. DR: drug removal. (B) The IC50 values for M397 cells at untreated, upon long-term drug exposure (46 days), and after long-term drug removal (treatment discontinued for 33 days), confirming the reverted cells are re-sensitized to BRAF inhibition.

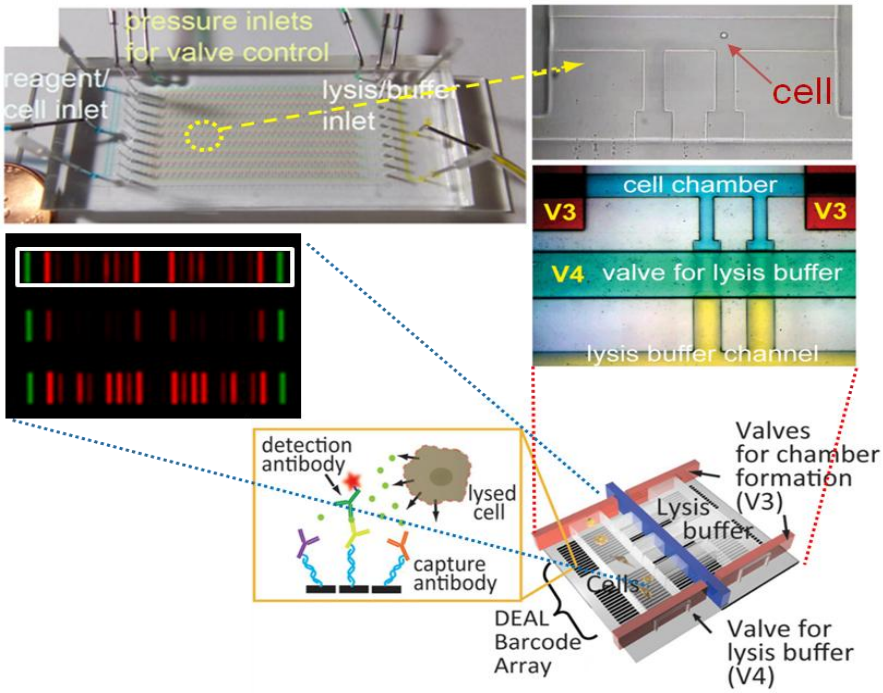

Fig. S15. The optical pictures of SCBC and its microchamber units: valves for chamber formation (red), valves for lysis buffer control (green), cell chamber compartment (blue), and lysis buffer reservoir (yellow) are delineated by food dyes. The sandwich immunofluorescence detection scheme with a scanned image is listed below the optical images. In the scanned image, the green stripes are used as alignment markers of a microchamber; each red stripe represents a functional protein measured and the fluorescence signal denotes the protein level from the single cells.

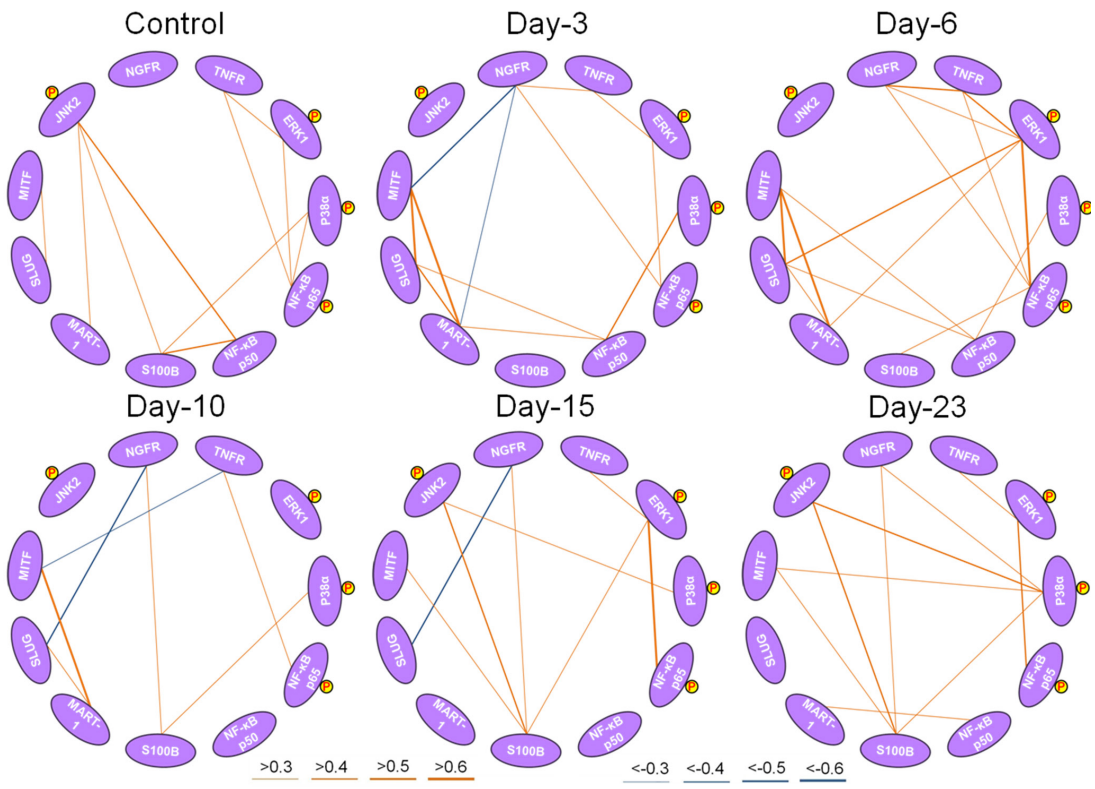

Fig. S16. Protein-protein correlation networks of M397 cells at different time points, extracted from SCBC data. The correlation (orange) / anti-correlation (blue) strength were reflected in the thickness of the edges (see keys).

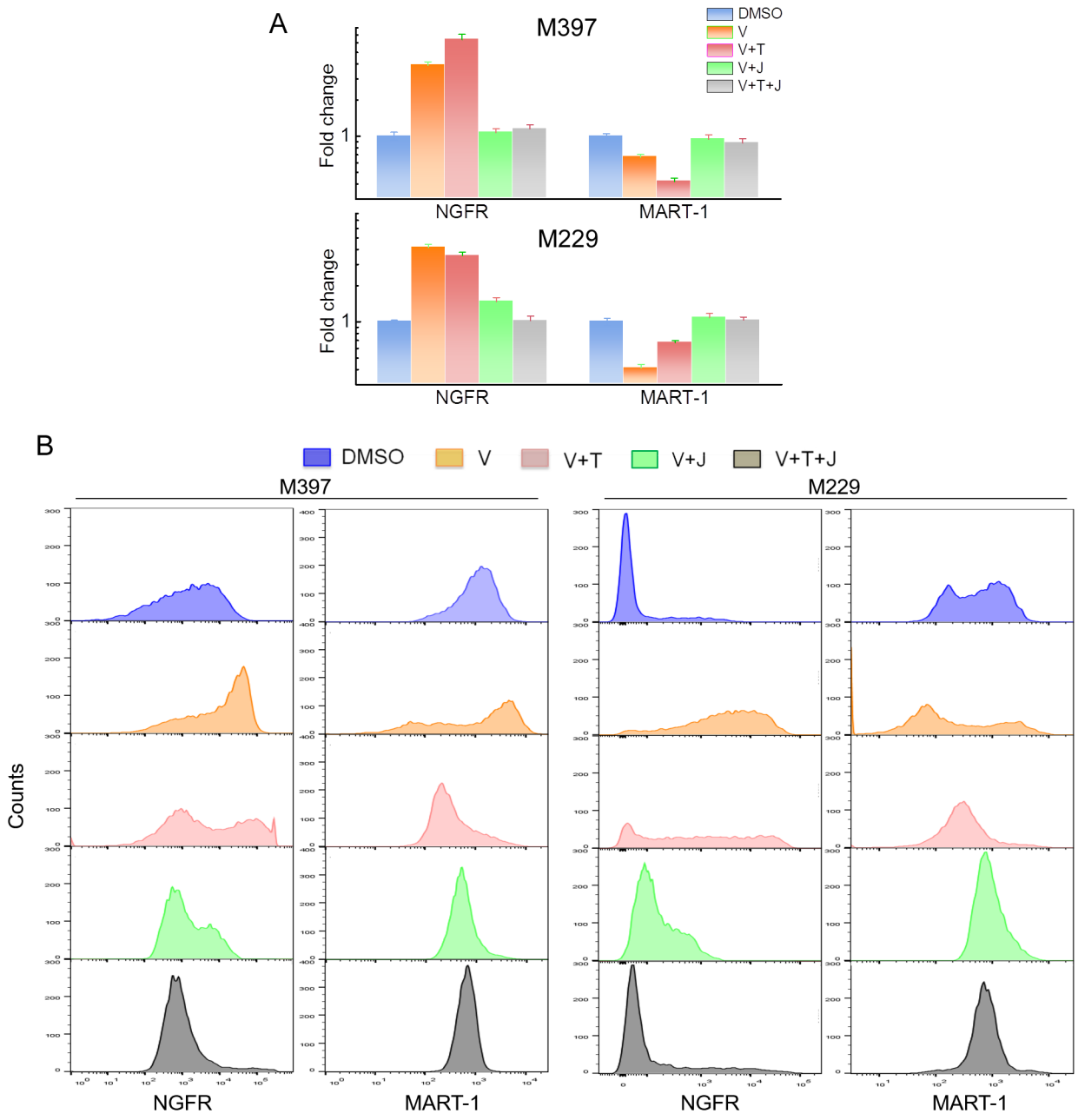

Fig. S17. Immunofluorescence and flow cytometry analyses of NGFR and MART-1 markers to BRAF inhibition. (A) Fold change of NGFR and MART-1 levels for mono- and combination therapies (23 days treatment) with respect to DMSO control on bulk M397 and M229 populations quantified by sandwich immunofluorescence assay. The predicted effective combinations (V+J and V+T+J) keep the MART-1 and NGFR levels unchanged, while V or V+T induces significant NGFR up-regulation and loss of MART-1 (error bars: ±SD). (B) Cell phenotype marker histograms from flow cytometry analysis of MART-1 and NGFR levels for mono- and combination therapies on both M397 (23 days drug treatment) and M229 (28 days drug treatment).

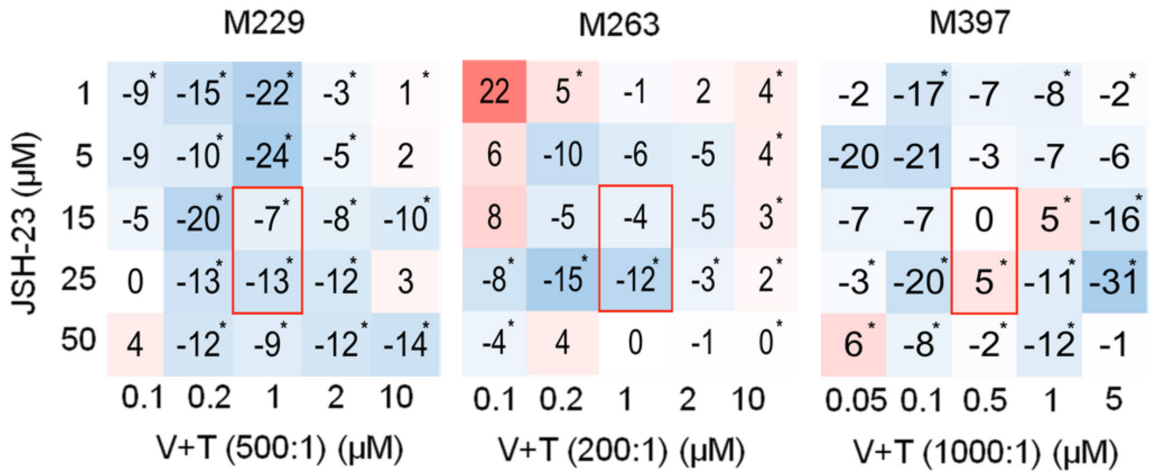

Fig. S18. Synergy effects of combining vemurafenib (V) and trametinib (T) with JSH-23 (J). Percentage of excess activity over that expected under the Bliss independence assumption for each of the various dose combinations. Red indicates synergy; blue indicates antagonism. The red boxes outline the concentration ranges used in the long-term clonogenic assays in Fig. 4. *p<0.05 under Student's t-test.

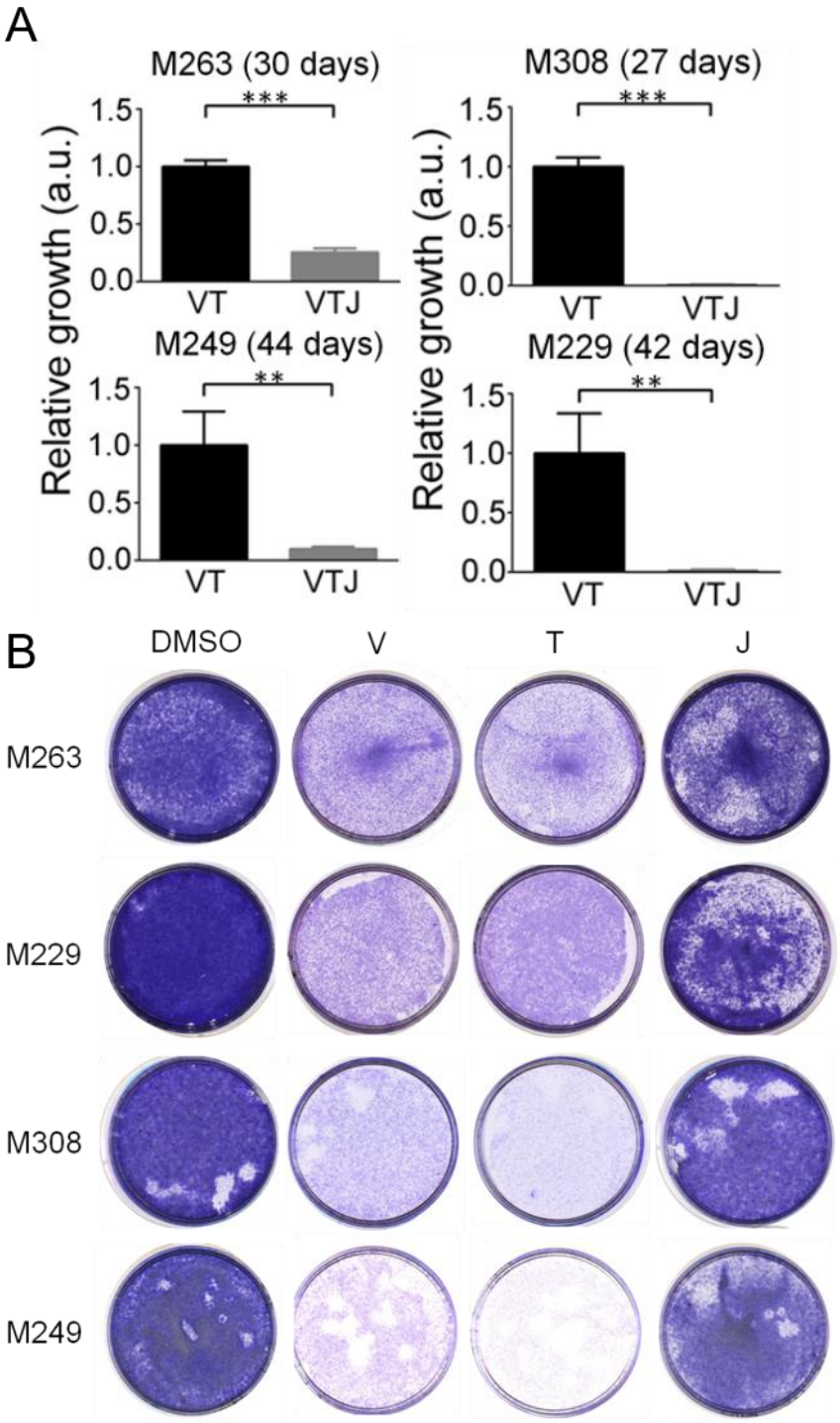

Fig. S19. Clonogenic assays for long-term combination therapy and short-term monotherapies in a cohort of melanoma cell lines. (A) Clonogenic assays of long-term drug treated samples were quantified using ImageJ software and normalized to V+T. The statistical significance is evaluated by Student's t-test. **p<0.005, ***p<0.0005. Error bars: ±SD). (B) The same doses used in long-term combination treatments were used for monotherapies here. No significant toxicity to the cells was observed for using JSH-23 alone (treatment time: M263, 7 days; M229: 11 days; M308: 10 days; M249: 7 days).

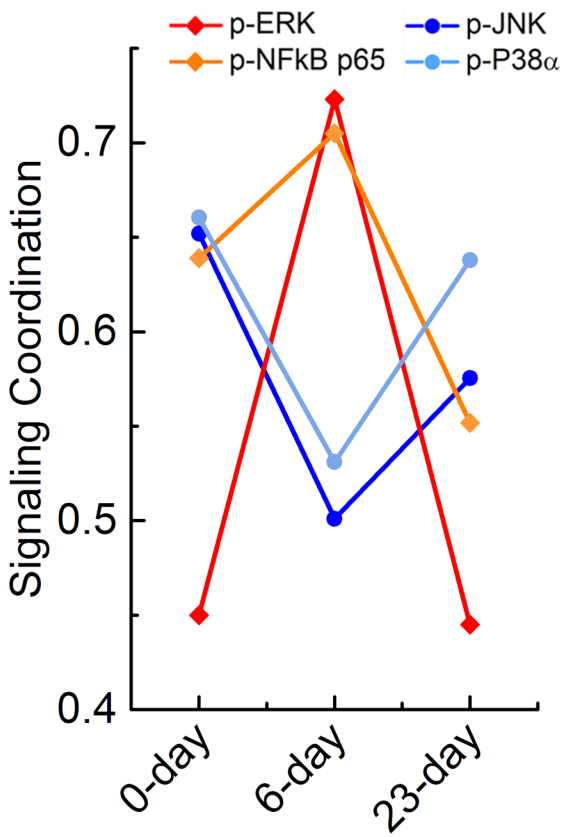

Fig. S20. Change in signaling coordination quantified as correlations between key functional proteins and the first principal component for control, day-6 (initiation of the adaptive transition), and day-23 (establishment of adaptive resistance). The up-regulation of JNK and p38α signaling axes is identified when the cells develop adaptive resistance to BRAFi.

Supplementary Tables

Table S1. Characterization of 18 melanoma cell lines used in this study, where 9 randomly selected cell lines from each cluster for transcriptomic studies are shadowed in red.

Cell line	Sensitivity	IC50 (nM)	Mutational Status	
M370	R	>10000	BRAFV600E mutant	**Cluster A**
M381	R	>10000	BRAFV600E mutant	
M410	R	3510	BRAFV600E mutant	
M233	R	>10000	BRAFV600E mutant 3 copies BRAF AKT1 amplification CCN31 amplification EGFR amplification CDKN2A deletion PTEN deletion	**Cluster B**
M238	S	243	BRAFV600E mutant 2 copies BRAF CDKN2A deletion PTEN deletion	
M255	I	1625	BRAFV600E mutant 2 copies BRAF AKT2 amplification CCND1 amplification EGFR amplification CDKN2A deletion	
M395	S	131	BRAFV600E mutant	
M406	S	645	BRAFV600E mutant	
M409	I	1018	BRAFV600E mutant	
M411	S	171	BRAFV600E mutant	
M229	S	282	BRAFV600E mutant 4 copies BRAF MITF amplification AKT1 amplification PTEN deletion	**Cluster C**
M263	I	839	BRAFV600E mutant 2 copies BRAF CDKN2A deletion	
M397	S	132	BRAFV600E mutant	
M399	I	1155	BRAFV600E mutant	
M403	S	450	BRAFV600E mutant	
M249	S	273	BRAFV600E mutant 3 copies BRAF MITF amplification AKT2 amplification PTEN deletion	**Cluster D**
M262	S	150	BRAFV600E mutant 2 copies BRAF AKT1 mutation&amp CDKN2A deletion	

M308	R	>10000	BRAFV600E mutant 3 copies BRAF MITF amplification AKT2 amplification EGFR amplification CDKN2A deletion	

Table S2. Color coded table comparing normalized median fluorescence intensity values for MART-1 and NGFR upon 3 days and 21 days of vemurafenib exposure with respect to DMSO control. The data are extracted from flow cytometry analysis (Fig. S2) across 18 cell lines. Fold changes are listed and color coded (red: increase, blue: decrease).

	MART1		NGFR	
Cell lines	**Vem 3d**	**Vem 21d**	**Vem 3d**	**Vem 21d**
M370	1.05	1.01	0.90	1.13
M381	0.89	1.07	1.04	1.56
M410	0.85	0.84	0.82	0.96
M233	0.94	0.66	1.05	7.20
M238	0.47	0.67	33.89	47.89
M255	0.29	1.13	1.51	2.07
M395	0.84	0.64	27.70	11.20
M406	0.87	0.87	2.04	4.85
M409	0.77	1.16	2.52	4.66
M411	0.70	0.77	5.98	26.00
M229	2.10	0.16	0.48	127.17
M263	2.15	2.25	7.38	6.10
M397	1.71	0.33	0.82	4.42
M399	5.04	2.79	4.04	1.54
M403	1.77	1.25	0.00	1.47
M249	1.61	1.88	0.05	1.82
M262	1.01	0.77	0.02	0.89
M308	0.89	0.60	6.50	27.03

Table S3. Complete chicken neural crest gene set list from Gallus Expression in situ Hybridization Analysis (GEISHA) (12)

Chick_neural_crest (GEISHA)		
AARS	HDAC2	PDGFD
ABCF2	HES1	PDGFRA
ACVR2B	HES5	PEBP1
ADAM12	HES6	PENK
ADAM33	HEY1	PGK1
ADAMTS1	HEY2	PITX2
ADAMTS3	HK2	PLEKHG1
AGR2	HNRNPM	POU3F4
AHCYL1	HOXA3	PTK7
ALK	HOXB7	RAC1
ALX1	HS2ST1	RARA
ANGPTL4	HS3ST3A1	RARB
ANK3	HTRA1	RAR-GAMMA2
ANKRD6	ID2	RCC2
ANXA6	IPO9	RELT
AP2A2	IREB2	RERE
ARHGAP15	ISL1	RET
ARHGAP28	KDM4A	RHOB
ASCL1	KIF4A	RHOU
AUTS2	KLF10	RND3
B-G	KTN1	ROBO1
BLNK	LAMA5	ROBO2
BMP4	LECT1	RSPO3
BMP7	LFNG	RXRA
BMPER	LGR4	SALL4
BTBD11	LIMS1	SEMA3D
BTG2	LMNB2	SEMA7A
CADM3	LMO4	SIX1
CDH11	LOC100858038	SIX4
CDH6	LOC420041	SLC7A3
CRABP1	LZTS1	SLIT1
CXCL14	MAFA	SMO
CXCR4	MAFB	SNAI1
CYP26C1	MAFK	SNAI2
DACH1	MAP3K5	SOX10
DACT2	MATN4	SOX2
DAD1	MCAM	SOX8
DKC1	MECOM	SOX9
DLL1	MEF2C	SPRY2
DLL4	MKRN1	SREBF2
DLX3	MMP2	STOX1
DLX5	MOXD1	TBX1
DRGX	MSX1	TBX3
DSC2	MSX2	TCF3
DSG2	MXI1	TFAP2A
EBF2	MYC	TIAM1
EDNRB	MYCN	TIAM2
EFNB2	NCOA1	TIMP2
EGR4	NES	TPD52L2
ELK3	NET1	TRIO
ENAH	NEUROD4	TSHZ2
EPCAM	NEUROG1	VSX1
ETS1	NHLH1	WIF1
EYA2	NKX2-5	WNT-1
FGF13	NOG	WNT16
FGF3	NOLC1	WNT8A
FGFR2	NR6A1	ZEB2
FGFR3	NRP2	ZIC1
FLT4	OLFM1	ZRANB1
FOXD3	OSBP2	
FRZB	PALLD	
FZD1	PAX3	
GATA1	PAX7	
GFRA2	PCDH15	
GLG1	PCDH18	
GTF2E2	PCDH8	

Table S4. GSEA enrichment across innate anti-PD-1 resistance (IPRES) signature at 3 days and 21 days of BRAFi exposure using averaged gene expression levels of the 3 plastic cell lines. NES stands for normalized enrichment score.

IPRES (M229_M263_M397)	3days			21 days			73days		
	NES	p-value	q-value	NES	p-value	q-value	NES	p-value	q-value
ANASTASSIOU_CANCER_MESENCHYMAL_TRANSITION_SIGNATURE	1.66	0	0.056	2.18	0.0001	0.0001	2.37	0.0001	0.0001
VECCHI_GASTRIC_CANCER_ADVANCED_VS_EARLY_UP	1.22	0.072	0.368	1.8	0.0001	0.002	1.73	0.0001	0.01
MAPKi_INDUCED_EMT	-1.1	0.301	0.301	1.61	0.003	0.003	1.93	0.0001	0.0001
LU_TUMOR_ENDOTHELIAL_MARKERS_UP	-1.36	0.097	0.17	0.99	0.471	0.626	1.33	0.102	0.214
LU_TUMOR_VASCULATURE_UP	-1.01	0.43	0.637	1	0.465	0.615	1.35	0.076	0.193
ROY_WOUND_BLOOD_VESSEL_UP	1.17	0.189	0.431	1.78	0.0001	0.003	1.98	0.0001	0.0001
post_op_woundhealing	-1.38	0.01	0.01	1.34	0.028	0.028	1.82	0.0001	0.0001
lef1_up.v1_up	-1.1	0.203	0.371	1.6	0.0001	0.005	1.53	0.001	0.019
MAPKi_INDUCED_ANGIOGENESIS	1.1	0.308	0.308	1.79	0.0001	0.0001	1.97	0.0001	0.0001
EP_BLOOD_VESS_DEVEL_DN_IN_R	-0.84	0.737	0.737	1.64	0.006	0.006	1.85	0.002	0.002
MISHRA_CARCINOMA_ASSOCIATED_FIBROBLAST_UP	-1.04	0.405	0.597	1.59	0.01	0.03	1.67	0.007	0.021
LIEN_BREAST_CARCINOMA_METAPLASTIC	1.19	0.18	0.392	1.76	0.0001	0.004	1.88	0.0001	0.001
CHARAFE_BREAST_CANCER_BASAL_VS_MESENCHYMAL_UP	-0.91	0.652	0.78	0.89	0.715	0.786	-1.18	0.111	0.399
MAHADEVAN_GIST_MORPHOLOGICAL_SWITCH	1.64	0.004	0.057	1.55	0.021	0.045	1.77	0.0001	0.006
WESTON_VEGFA_TARGETS_6HR	1.42	0.024	0.21	1.86	0.0001	0.001	2.07	0.0001	0.0001
WESTON_VEGFA_TARGETS_12HR	1.76	0.0001	0.021	1.91	0.0001	0.0001	2.01	0.0001	0.0001
MS_RESP_TO_WOUNDING_UP_IN_MAPKi_aPDL1_NR	-1.53	0.004	0.004	1.1	0.304	0.304	1.41	0.042	0.042
POOLA_INVASIVE_BREAST_CANCER_UP	-2.04	0.0001	0.0001	-1.17	0.058	0.402	1.3	0.02	0.238
YE_METASTATIC_LIVER_CANCER	-1.17	0.219	0.391	-1	0.419	0.658	0.85	0.687	0.856
KARAKAS_TGFB1_SIGNALING	-0.92	0.579	0.772	1.19	0.208	0.327	1.3	0.134	0.237
JAEGER_METASTASIS_DN	1.23	0.047	0.351	1.83	0.0001	0.001	1.58	0.0001	0.049
MS_RESP_TO_HYPOXIA_UP_IN_MAPKi_aPDL1_NR	-0.94	0.541	0.541	1.45	0.033	0.033	1.53	0.027	0.027
LU_TUMOR_ANGIOGENESIS_UP	-0.78	0.803	0.938	1.2	0.2	0.311	1.14	0.257	0.436
MAINA_VHL_TARGETS_DN	-0.87	0.668	0.839	1.26	0.183	0.251	1.49	0.032	0.088
HARRIS_HYPOXIA	-1.04	0.363	0.591	1.62	0.0001	0.023	2.01	0.0001	0.0001
JEON_SMAD6_TARGETS_UP	1.74	0.0001	0.026	1.79	0.0001	0.002	1.68	0.003	0.018

Table S5. Cell state composition measured by flow cytometry across time, while being with or without BRAF inhibition. DN – double negative mesenchymal-like state (NGFR-/MART-1-), NC – neural crest-like state (NGFR+/MART-1-), DP – double positive plastic state (NGFR+/MART-1+), melanocytic state (NGFR-/MART-1+).

		NGFR+					NGFR-				
		Cycle	DN	NC	Melanocytic	DP	Cycle	DN	NC	Melanocytic	DP
M397	treatment naïve condition	0	0.0%	2.4%	0.0%	97.6%	0	0.5%	0.0%	99.5%	0.0%
		1	0.3%	29.4%	0.7%	69.7%	1	3.3%	7.7%	32.1%	57.0%
		3	0.2%	28.1%	0.9%	70.8%	3	2.4%	22.0%	18.1%	57.5%
		6	0.3%	34.8%	2.9%	62.0%	6	3.3%	30.0%	17.7%	49.0%
		10	0.3%	34.0%	2.5%	63.2%	10	1.4%	26.9%	11.7%	60.0%
		15	0.4%	22.3%	3.8%	73.5%	15	2.9%	11.7%	31.7%	53.7%
	drug treatment condition	0	0.0%	2.4%	0.0%	97.6%	0	0.5%	0.0%	99.5%	0.0%
		1	0.2%	9.1%	1.3%	89.6%	1	2.1%	2.9%	55.3%	39.7%
		3	0.1%	15.3%	1.7%	82.9%	3	1.6%	8.2%	33.0%	57.3%
		6	0.2%	30.1%	4.1%	64.0%	6	16.3%	14.9%	18.2%	50.6%
		10	30.1%	44.0%	3.8%	22.1%	10	50.7%	13.9%	19.4%	16.0%
		15	65.2%	27.7%	3.7%	3.4%	15	82.0%	11.9%	4.4%	1.7%
M229	treatment naïve condition	0	0%	59%	0%	41%	0	39%	0%	61%	0%
		7	20%	49%	19%	12%	7	34%	10%	55%	2%
		10	19%	46%	24%	12%	10	17%	12%	69%	2%
		15	38%	37%	20%	6%	15	28%	12%	58%	1%
		20	29%	25%	40%	5%					
	drug treatment condition	7	6%	68%	3%	23%	7	10%	27%	35%	28%
		16	2%	82%	1%	16%	16	5%	51%	8%	37%
		38	10%	83%	0%	6%	38	25%	69%	1%	5%
		60	17%	72%	3%	8%	60	32%	56%	2%	11%
		71	38%	61%	0%	1%	71	68%	26%	5%	1%

Table S6. Phenotype proportion for M397 and M229 unsorted cells under drug treatment condition.

Cell Line	Cycle	DN	NC	Melanocytic	DP
M397	0	0%	7%	17%	76%
	2.3	0%	9%	25%	66%
	7	1%	44%	8%	46%
	14.3	53%	39%	1%	7%
	20.6	64%	32%	0%	4%
	22	76%	20%	0%	4%
	26	74%	21%	5%	1%
M229	0	6%	7%	76%	12%
	11	2%	28%	25%	46%
	21	2%	63%	2%	32%
	30	1%	62%	2%	34%
	38	3%	75%	1%	22%
	60	25%	59%	16%	0%
	71	42%	52%	5%	1%

Table S7. The sequences of the oligonucleotides used in the protein immunoassays. All oligonucleotides were synthesized by Integrated DNA Technology (IDT) and purified via high performance liquid chromatography (HPLC). The DNA coding oligomers were pre-tested for orthogonality to ensure that cross-hybridization between non-complementary oligomer strands was negligible (<1% in photon counts).

	DNA sequence used for pattering ssDNA microarray
A	5'-AAAAAAAAAAAAAATCCTGGAGCTAAGTCCGTA-3'
B	5'-AAAAAAAAAAAAAGCCTCATTGAATCATGCCTA-3'
C	5'-AAAAAAAAAAAAAGCACTCGTCTACTATCGCTA-3'
D	5'-AAAAAAAAAAAAAATGGTCGAGATGTCAGAGTA-3'
E	5'-AAAAAAAAAAAAAATGTGAAGTGGCAGTATCTA-3'
F	5'-AAAAAAAAAAAAAATCAGGTAAGGTTCACGGTA-3'
G	5'-AAAAAAAAAAAAAGAGTAGCCTTCCCGAGCATT-3'
H	5'-AAAAAAAAAAAAAATTGACCAAACTGCGGTGCG-3'
I	5'-AAAAAAAAAAAAAATGCCCTATTGTTGCGTCGGA-3'
K	5'-AAAAAAAAAAAAAATAATCTAATTCTGGTCGCGG-3'
L	5'-AAAAAAAAAAAAAGTGATTAAGTCTGCTTCGGC-3'
M	5'-AAAAAAAAAAAAAGTCGAGGATTCTGAACCTGT-3'
N	5'-AAAAAAAAAAAAAGTCCTCGCTTCGTCTATGAG-3'
	Complementary ssDNA Sequence for antibody conjugation
A'	5'NH3-AAAAAAAAAAAAATACGGACTTAGCTCCAGGAT-3'
B'	5'NH3-AAAAAAAAAAAAATAGGCATGATTCAATGAGGC-3'
C'	5'NH3-AAAAAAAAAAAAATAGCGATAGTAGACGAGTGC-3'
D'	5'NH3-AAAAAAAAAAAAATACTCTGACATCTCGACCAT-3'
E'	5'NH3-AAAAAAAAAAAAATAGATACTGCCACTTCACAT-3'
F'	5'NH3-AAAAAAAAAAAAATACCGTGAACCTTACCTGAT-3'
G'	5'NH3-AAAAAAAAAAAAAAATGCTCGGGAAGGCTACTC-3'
H'	5'NH3-AAAAAAAAAAAAACGCACCGCAGTTTGGTCAAT-3'
I'	5'NH3-AAAAAAAAAAAAATCCGACGCAACAATAGGGCA-3'
J'	5'NH3-AAAAAAAAAAAAACCTGCTCGACAACTAGAAGA-3'
K'	5'NH3-AAAAAAAAAAAAACCGCGACCAGAATTAGATTA-3'
L'	5'NH3-AAAAAAAAAAAAAGCCGAAGCAGACTTAATCAC-3'
M'	5'Cy3-AAAAAAAAAAAAAACAGGTTCAGAATCCTCGAC-3'
N'	5'NH3-AAAAAAAAAAAAACTCATAGACGAAGCGAGGAC-3'

Table S8. List of antibodies used for the SCBC multiplex protein assays.

Antibody	Manufacture
Human NGFR DuoSet	R&D DY367
Human sTNF DuoSet	R&D DY225
Human S100B Mab Mouse IgG2A	R&D MAB1820
S100B Rabbit mAb	Cell Signaling 9550
Melan-A Monoclonal	Sigma-Aldrich M6570
Human Melan-A/MART-1 Sheep IgG	R&D AF8008
Human Phospho-JNK2 DuoSet	R&D DYC2236
Human MITF Goat IgG	R&D AF5769
MITF	abcam ab80651
Human/Mouse/Rat Phospho-ERK1	R&D DYC1825
Human NFκB1 Mouse IgG	R&D MAB2697
NFκB1 p105/p50	Cell Signaling 3035
Human/Mouse NFκB p65 Mouse IgG2B	R&D MAB5078
Phospho-NFκB p65 Rabbit mAb	Cell Signaling 4025
Phospho-IκB alpha (Ser32) ELISA Kit	Cell Signaling 7343
Phospho-p38 alpha DuoSet	R&D DYC869B
Slug (SNAI2) mouse IgG	Sigma-Aldrich SAB1412527
Slug Rabbit mAb	Cell Signaling 9585

Dataset S1. Kinetic RNA-seq data of the 9 randomly selected melanoma cell lines. (See Excel file attached).